

Internal Letter



Rockwell International

NASA-14600

Date 3 November 1977

SEH-ITA-77-245

CR160146

TO: M. E. Wilson/M. Harthun  
D/390 AC85 D/390 AC78  
Space Division/Downey

FROM: W. Rochelle/B. Kimbrough/  
J. Gallegos/M. Hale/R. Miller  
(G. W. Mauss, Supervisor)  
D/115, 0411-ZC01

Subject: Prediction of In-Depth Gap Heating Ratios from Wing Glove  
Model Test Data

ORIGINAL FILED IN  
CR 160146

References:

1. IL from G. W. Mauss to R. Watanabe/M. Harthun, subject "Quick-Look Report of Silfrax Wing Glove Model Calibration Test in JSC 10MW Arc-Jet Facility," Rockwell International IL SEH-ITA-77-114, May 12, 1977.
2. IL from W. C. Rochelle to R. Watanabe/M. Harthun, subject "High  $\Delta P$ , Wing Glove Test Program - Summary Report of Cold Wall Calibration Test Results in JSC 10MW Arc-Jet Facility," Rockwell International IL SEH-ITA-77-137, June 7, 1977.
3. IL from W. C. Rochelle/J. J. Gallegos to R. Watanabe/M. Harthun, subject "High  $\Delta P$ , Wing Glove Test Program - Summary Report of RSI Gap Model Test Results in JSC 10MW Arc-Jet Facility," Rockwell International IL SEH-ITA-77-177, 4 August 1977.
4. Fesler, L. W., "TPS Multidimensional Heat Conduction S/370 Computer Program XF0031 - User's Guide," Rockwell International SD75-SH-0139, August 1975.
5. Wilson, M. E., "Space Shuttle Program - Thermodynamic Design Data Book - Thermal Protection System," Rockwell International SD73-SH-0226, Vol. 2C, July 1977.
6. IL from W. C. Rochelle to R. Watanabe/M. Harthun, subject "Quick-Look Report of Gap/Step Model Calibration Tests in Channel Nozzle of JSC 10MW Arc-Jet Facility," Rockwell International IL SEH-ITA-77-185, 12 August 1977.
7. IL from W. C. Rochelle/J. J. Gallegos/M. Hale to R. Watanabe/M. Harthun, subject "Summary of Test Results from 2.0 and 1.0 Inch RSI Gap/Step Models in JSC 10MW Arc-Jet Facility," Rockwell International Internal Letter to be published November 1977.

Summary

In-depth gap heating ratios,  $q(z)/q_{ref}$ , were predicted down RSI tile sidewalls based on temperature measurements obtained from the JSC arc-jet Wing Glove model tests. The objectives of the study were to develop gap heating ratios which resulted in the best possible fit of test data and to produce a set of engineering verification heating ratios similar in shape to one another which could be used at various body points on the Orbiter during reentry. The Rockwell TPS Multidimensional Heat Conduction Program (XF0031) was used to perform 3-D thermal analyses using a 3.0 in. thick section of a curved RSI tile with 283 nodal points. The results of the correlation with test data showed that the predicted heating ratios were significantly higher down in the gap than the zero pressure gradient values for T/C stacks 39 and 38 on the Wing Glove model. For stack 37 (in a low pressure region), the baseline heating ratio overpredicted the temperature data. This analysis, which showed that the heating ratios were a strong function of the product of pressure and pressure gradient, will be used to compare with recent Gap/Step and Ames Double Wedge test/analysis results in the effort to identify the Orbiter gap response to High  $\Delta P$  flight environment.

(NASA-CR-160146) PREDICTION OF IN-DEPTH GAP HEATING RATIOS FROM WING GLOVE MODEL TEST DATA (Rockwell International Corp., Downey, Calif.) 57 p HC A04/MF A01 CSCL 20D N79-20068 Unclas G3/02 18331

ORBITER WING GLOVE  
RESEARCH REPORT

## 1.0 Introduction

A series of three test programs (References 1-3) was performed at the NASA/JSC 10MW Arc Jet Facility using a model of the Orbiter Wing Glove region. This model was located some 25 in. downstream of a 40 in. diameter conical nozzle at the facility. During the third test program of the series (Reference 3), in-depth temperature measurements were obtained at a number of stacks of thermocouples located in the gaps of the model. A primary result of this test program showed that when filler was installed in the longitudinal (stagnation line) gap the temperatures in the circumferential gap increased some 100-400°F above those for tests with no gap fillers. As a result, the data from the five filled stagnation line gap tests (C-188, 189, 190, 194, and 195) was used to correlate with thermal math model predictions. Tests C-188, 189, and 195 were high pressure tests, Test C-194 was a moderate pressure test and Test C-190 was a low pressure test as seen in the surface pressure plot of Figure 1. Data from three thermocouple stack locations (39, 38, and 37) as seen in Reference 3 was used for each of the five test cases. The principal surface data including pressure, pressure gradient, and temperature near each of these stacks and the test conditions for all five cases is presented in Table I.

The TPS Multidimensional Heat Conduction Program (XF0031) described in Reference 4 was used to develop an analytical math model of one quarter of an RSI tile. Both the derived value of heating ratio,  $q(z)/q_{ref}$ , and the original zero pressure gradient (baseline) value obtained from Ref. 5 were used in the analysis. Reference heating rates and surface pressures at the top of each stack were input as a function of time for each arc-jet test. Engineering verification heating ratios were developed that yielded smoothed curves, roughly parallel to each other, that were a function of the product of surface pressure and pressure gradient. The remainder of this document presents the details of the analytical model developed and the correlation with the Wing Glove model test data.

## 2.0 Analytical Model

### 2.1 Basic Description of Model

A 283 node 3-D model of a one-quarter curved RSI tile as shown in Figure 2 was developed and analyzed with the Rockwell XF0031 thermal analyzer program. With this program the solution to the 3-D heat conduction partial differential equation is obtained by the finite difference method. The method used to integrate the heat flow equation for all of the cases analyzed was the Crank-Nicolson method, which is based on a "mid" difference implicit numerical analysis technique.

The model used in the analysis had an LI300 RSI depth of 3.0 in. plus a 0.015 in. coating, 0.16 in. SIP thickness, and aluminum thickness ( $\bar{t}$ ) of 0.063 in. The properties of these four materials (RSI, coating,

SIP, and Al 2024) were input to the analytical model as either constant, a function of temperature only, or as a function of both temperature and pressure, as obtained from Ref. 5. The bottom side of the aluminum structure was driven at a temperature corresponding to that measured for each test. It was assumed the Silfrax tile across the circumferential gap from the RSI tile had the same properties as the RSI tile.

In the analytical model the specific heat and thermal conductivity of the 0042 coating and Al 2024 structure were input as a function of temperature only. The RSI specific heat was also input as a function of temperature only while the RSI and SIP thermal conductivity were input as a function of pressure and temperature. The surface pressures at each stack were input as a function of test time. The SIP specific heat, coating emissivity, and the density of all materials were input as constant values.

The radiation view factors down the gap were input from calculations obtained from the 2-D Cross-String Method Program. This program was written by Rockwell for use on the Hewlett-Packard 9830A Mini-Computer. The script-F radiant interchange factors across each enclosure were computed by the XF0031 Program by solving a system of linear algebraic equations, based on the emissivity, nodal surface areas and input view factors.

The temperatures and materials on either side of the gaps were assumed equal to each other at corresponding depths (thermal symmetry). The surface emissivity of all surface nodes was assumed to be 0.85. The initial temperature of all nodes was taken to be 80°F. This temperature was also assumed to be the sink temperature inside the vacuum chamber for all surface nodes radiating to the sink. The most sensitive parameters in the analysis were the heating ratio down the walls and the reference heating rate at each T/C stack investigated. These items are discussed in detail in the next section.

## 2.2 Heating Ratio and Reference Heating Rate

The Wing Glove region upon which this thermal analysis was performed included the distance along the circumferential gap from thermocouple stacks 43, 39, 38, 37, to 34 as seen in Reference 3. The main emphasis of the analysis was upon stacks 39, 38, and 37. Stacks 43 and 34 were at the junction of the circumferential and longitudinal gaps. Stack 43 was in a stagnation region, and stack 34 was in a separated flow region.

As noted in Figure 2, two specific models of the T/C stacks were used depending on which stack was being investigated: 1) Model 38-39-43 or 2) Model 38-37-34. The stack 39 analysis used the first model, the stack 37 analysis used the second model, and the stack 38 analysis used both models. When the analysis

was performed for stacks 38 or 39 the reference heating rate at stack 38 was input at nodes 11, 12 and 13 (Refer to Figure 2), the reference heating rate at stack 39 was input at nodes 6, 7, and 8 and the reference heating rate at stack 43 was input at nodes 1, 2, and 3. When the analysis was performed at stack 37, (Model 38-37-34) the reference heating rate at stack 37 was input at nodes 6, 7, and 8, the reference heating rate at stack 38 was input at nodes 11, 12, and 13, and the reference heating rate at stack 34 was input at nodes 1, 2, and 3.

The derived heating ratio  $q(z)/q_{ref}$  was applied down the walls facing the circumferential gap. The same heating ratio that was applied under node 3 was applied down the wall facing the longitudinal gap for lack of better definition. When stack 38 or 39 was being evaluated, the derived value of  $q(z)/q_{ref}$  at stacks 38 and 39 was applied down nodes 706, 712, 718..., and nodes 705, 711, 717..., respectively. At the same time, the derived values of  $q(z)q_{ref}$  at stack 39 were input to stack 43 (nodes 704, 710, 716...). A different value of heating ratio was not input to this stack because by the time of tests C-188 et al nearly all of the thermocouples near stack 43 had burned through, precluding any possibility of obtaining any comparison with temperature in this region. Where stack 37 was being evaluated (Model 38-37-34) the derived value  $q(z)/q_{ref}$  was input down stack 38 and the baseline value was input down stack 37 and 34 (in addition to being input down the upper longitudinal gap).

The reference heating rate at the surface of each of the three thermocouple stacks analyzed (37, 38, and 39) for each of the five tests is listed as a function of test time in Table II. In order to calculate this heating rate the ratio of  $T/T_{S=0}$  at each stack was determined by using Figure 3 which shows  $T/T_{S=0}$  as a function of enthalpy for two general locations: 1)  $S=-3.0$  in. and 2)  $S=3.0$  in.,  $S=7.3$  in., and  $S=7.9$  in. The  $-3.0$ ,  $3.0$  and  $7.9$  in. locations were from the cold wall model tests of Reference 2, and the  $7.3$  in. location was from the Silfrax model tests of Reference 1. Although the data for three values of  $S$  are superimposed on the upper curve one line may be faired through all the data points.

By observation of Figure 4 it may be seen that the value of  $T/T_{S=0}$  is approximately the same at all three of the locations in Figure 3. Hence at each enthalpy associated with the five cases, the upper curve of Figure 3 was used to obtain  $T/T_{S=0}$  for stack 39. These ratios are tabulated in Table I along with the temperatures. Since  $S=0$  at stack 38,  $T=T_{S=0}$  at this stack. The value of  $T_{S=0}$  at stack 38 was taken to be  $T_{1A}$  (assumed constant across the model) and was obtained from the facility printout as a function of time. For this temperature (at stack 38) the surface heating rate was computed as  $q_{ref} = \epsilon \sigma T_w^4$  ( $\epsilon = .85$ ) in Table II. For stacks 37 and 39, the ratio  $T/T_{S=0}$  was multiplied by the temperature at stack 38 to obtain  $T_{37}$  and  $T_{39}$  (see Table I), and the corresponding value of  $q_{ref}$  was calculated at these temperatures.

When stack 37 was analyzed, the thermal model included stacks 38, 37, and 34. To obtain  $T/T_S=0$  at stack 34, Figure 4 was used to interpolate the ratio  $T/T_S=0$  using a value of  $S=-5.7$  in. In the same manner, when stack 39 was analyzed (model containing stacks 38, 39, and 43), Figure 4 was used to interpolate the ratio  $T/T_S=0$  using a value of  $S=+5.7$  in. No surface data was obtained close to these points on any of the three test models (Silfrax, cold wall or RSI) and consequently was not plotted in Figure 4.

### 3.0 Results from Analysis

The results from this Wing Glove model analysis will be discussed in two general categories: 1) Best-Fit Heating Ratio and 2) Engineering Verification Heating Ratio. Category 1 contained the majority of the emphasis of this study as it required considerable iterations in most cases to obtain the heating ratio that would produce the best match of temperature data within schedule constraints.

#### 3.1 Best Fit Heating Ratio

The original Orbiter baseline gap heating ratio was adjusted upward at each nodal depth down to 3 in. in an attempt to match the temperature within 20-30°F at each thermocouple depth for stacks 39 and 38. At stack 37, because of the combined low pressures and pressure gradients, only the baseline value of heating ratio was used. This heating ratio consistently overpredicted the side wall temperature response at this location, possibly because of the presence of nearly separated flow in this region.

In Figures 5-9 the best-fit heating ratios have been used to correlate with temperature data at T/C stack 39 for Tests C-188, 189, 194, 195, and 190, respectively. Tests C-188, 189, and 195 were for a high stagnation pressure ( $\sim 22-23$  PSF) case, Test C-194 was for a moderate ( $\sim 16$  PSF) pressure case, and Test C-190 was for a low pressure ( $\sim 9$  PSF) case as seen in Table I and Figure 1. The principal time investigated for correlation with data was 600 sec. for all cases except C-194 which was 500 sec. In addition to these times shown in Figures 5-9, data for additional times (100, 200, 300, 400, and 800 sec.) are plotted in some of the figures. It may be seen that in most cases the predicted values at 600 sec. (500 sec. for C-195) are within 20-30°F of the test data.

Figures 10-14 present the temperatures at stack 38 using the best-fit heating ratios for Tests C-188, 189, 195, 194, and 190, respectively. The maximum temperatures in the gap at this stack are some 400-500°F lower than at stack 39. This stack had two extra thermocouples to correlate with the predictions. For practically all points on all cases except the low pressure case (C-190) the predicted temperature agreed within 20-30°F of the test data for the 600 and 500 sec. times. It was determined for C-190 that the best-fit heating ratio curve was actually lower than the baseline curve; hence the baseline curve is shown in Figure 14 for comparison with the data.

The temperatures at stack 37 are shown plotted in Figures 15-19 using the zero pressure gradient  $q(z)/q_{ref}$  for Tests C-188, 189, 195, 194, and 190, respectively. In this low pressure, moderate pressure gradient region it was seen that the baseline heating ratio over predicted the data by as much as 200°F in some cases. A faired line through the data would be nearly parallel to the predicted temperatures for most of the cases for stack 37. The uncertainty in the measured surface temperature (from which  $q_{ref}$  was based) in this region could have contributed to some of the lack of correlation at this stack. No "best-fit" heating ratio was used for this stack because of schedule constraints on the analysis.

The actual heating ratios used in this best-fit analysis are shown in Figure 20 for stacks 38 and 39. There is one curve with the baseline value used for stack 38 for Test C-190; this curve was also used for all of the stack 37 cases. An additional curve is shown for comparison purposes for case C-190 (C-190V) for stack 38 which is lower than the baseline value which actually gave a better fit to the data. All of the letter designations next to the case number in Figure 20 denote the iteration number used to obtain the best fit to the data.

It may be noted in Figure 20 that a value of  $P\Delta P/\Delta X$  is listed after each case number. There is an approximate correlation of heating ratio with this product, although there may be at least a 10% scatter in determining this product. For each stack 39 and 38 there appears to be a definite correlation of  $q(z)/q_{ref}$  with  $P\Delta P/\Delta X$  as seen in Figures 21 and 22, respectively. For location 38 (lower pressure) the heating ratio drops off considerably at low values of  $P\Delta P/\Delta X$  while for location 39 (higher pressure) the heating ratio is more linear at low values of  $P\Delta P/\Delta X$ .

### 3.2 Engineering Verification Heating Ratio

From Figure 20 it may be seen that several of the heating ratio curves tend to overlap each other. This is because of the attempt to achieve a close fit to experimentally measured temperatures that could be off at least 3-5% (as much as 50-80° at  $Z=0.1$  in. and 20-30°F at  $Z=2.375$  in.). Also, all of the curves in Figure 20 probably have at least a 10% error in the product  $P\Delta P/\Delta X$ . The top three curves of stack 39 and 38 (Cases C-188, 189, and 195) can be represented by a single heating ratio curve that will adequately predict temperatures at each thermocouple location.

In this manner a set of "engineering verification" curves was developed at each stack which were approximately parallel to each other and would not overlap at each stack. One of these curves was developed for all three cases (C-188, 189, and 195). These curves were all designed to at least predict or overpredict all thermocouple measurements. Figures 23 and 24 present these smoothed heating ratio curves at stack 39 and 38, respectively. Again the curve for stack 38, Test C-190 is the baseline, or zero pressure gradient curve.

Figure 25 shows the verification heating ratios plotted as a function of  $P\Delta P/\Delta X$  for stacks 38 and 39. Only two points are shown for stack 38 since the third point is the baseline value for Case 190 shown in Figure 24. This value is actually higher than C-194 (see Figure 24) at low values of Z and then drops to zero at  $Z=0.40$  in. From Figure 25 it may be seen that the heating ratios have a higher slope for stack 38 than for stack 39. This trend is consistent with the best-fit heating ratios of Figures 21 and 22, although there is some scatter in these "non-smoothed" heating ratio curves.

The comparison of predicted temperatures with Wing Glove model data using the engineering verification heating ratios are shown in Figures 26-40. Stack 39 comparisons are shown in Figures 26-30, stack 38 comparisons are shown in Figures 31-35, and stack 37 comparisons are shown in Figures 36-40 for Cases C-188, 189, 195, 194, and 190, respectively. In all of these figures only the comparison at 600 sec. (500 sec. for Test C-195) is shown. For stack 38 two curves are shown - for model 38-38-43 and model 38-37-34 - in order to assess the effects of lateral conduction on the temperature predictions.

A comparison of the temperatures predicted using the engineering verification heating ratios with the test data is shown in Figures 41-46 as a function of test time of the arc jet. Figures 41, 42, and 43 present the comparison at stack 39 for Cases C-195, 194, and 190, respectively. Figures 44, 45, and 46 show the comparison at stack 38 for Cases C-195, 194, and 190, respectively. It may be seen that there is better agreement at stack 38 than at stack 39, especially for the temperatures at  $Z=0.1$  in. For stack 39 the data was higher than the predictions during the initial 100 sec. For Test C-190 there was an early abort and then a restart which caused the higher initial temperatures (see Figure 54). The in-depth predictions were either close to the data or conservative with respect to it for all cases with the exception of Test 190 because of the restart.

#### 4.0 Conclusion

This document has presented a correlation of predicted temperatures with RSI Wing Glove model test data using derived values of in-depth gap heating ratios. Best-fit heating ratios were used with a number of iterations to produce a very close correlation with the data. Smoothed curves (engineering verification) were also developed that were similar in shape to each other and were conservative with respect to the data. It was seen that all of the heating ratios correlated well with the product of pressure and pressure gradient (low ratios for low  $P\Delta P/\Delta X$  and high ratios for high  $P\Delta P/\Delta X$  for all values of Z). The results of this

analysis will be used to make flight predictions of heating in the tile gaps at various Orbiter body points and will also be used to compare with recent arc-jet Gap/Step (flat plate) model data (References 6 and 7) and with data from the NASA/Ames Double Wedge Test Article high  $\Delta P$  tests.

TPS Analysis Unit  
Integrated Thermal Analysis  
Shuttle Engineering  
Field Operations, Houston

cc: H. H. Battley D/115, ZC01 *HHB*  
C. Blumer D/390, AC78  
J. J. Gallegos D/115, ZC01 *JG*  
W. M. Hale D/115, ZC01 *MH*  
B. Kimbrough D/115, ZC01 *BK*  
J. E. Lundgren D/390, AC78  
G. W. Mauss D/115, ZC01 *Gum*  
G. McIntyre D/390, AC78  
C. R. Miller D/115, ZC01 *C.R.M.*  
W. C. Rochelle D/115, ZC01 *WCR*  
C. L. Statham D/115, ZC01  
R. Watanabe D/390, AC78  
N. F. Witte D/390, AB83  
L. R. Johnson D/390, AC78  
S. A. Fung D/390, AC78  
W. E. Neuenschwander D/390, AC85  
P. C. Merhoff D/390, AC85

ORIGINAL PAGE IN  
OF FOUR QUARTERS

TABLE I. TEST CONDITIONS FOR WING GLOVE MODEL CASES ANALYZED

TEST TIME NO.	$\dot{m}$ (LB/SEC)	I (AMPS)	$h_b$ (BTU/LB)	$P_{S^{**}}$ (PSF)	$T_{1A^+}$ (°F)	$P_{39}$ (PSF)	$\frac{\Delta P}{\Delta X}$ (PSF/IN)	$P \frac{\Delta P}{\Delta X}$ (PSF <sup>2</sup> /IN)	$\frac{T}{T_{S=0}}$	$T_{39}$ (°F)	$P_{38}$ (PSF)	$\frac{\Delta P}{\Delta X}$ (PSF/IN)	$P \frac{\Delta P}{\Delta X}$ (PSF <sup>2</sup> /IN)	$\frac{T}{T_{S=0}}$	$T_{38^{++}}$ (°F)	$P_{37}$ (PSE)	$\frac{\Delta P}{\Delta X}$ (PSF/IN)	$P \frac{\Delta P}{\Delta X}$ (PSF <sup>2</sup> /IN)	$\frac{T}{T_{S=0}}$	$T_{37}$ (°F)
C-188 599	1.032	1292	1754	22.30	1429	18.8	2.7	50.8	1.18	1686	10.1	3.1	31.3	1.0	1429	2.8	1.6	4.5	0.76	1086
C-189 599	0.960	1622	2340*	23.30	1511	19.7	2.8	55.2	1.17	1768	10.4	3.1	32.2	1.0	1511	3.2	1.6	5.1	0.75	1133
C-190 596	0.258	1491	5183*	8.90	1811	7.8	1.2	9.4	1.09	1974	3.4	1.1	3.7	1.0	1811	1.1	0.4	0.4	0.706	1279
C-194 599	0.559	1942	3896	16.43	1737	13.9	2.1	29.2	1.12	1945	6.7	2.0	13.4	1.0	1737	2.0	1.1	2.2	0.72	1251
C-195 499	0.894	1942	2713	22.73	1624	19.5	2.8	54.6	1.16	1884	10.4	3.0	31.2	1.0	1624	3.0	1.7	5.1	0.74	1202

NOTE: \*  $h_b$  LISTED OBTAINED FROM OTHER TESTS WITH SAME TEST CONDITIONS: HEATER WATER T/C IMPERATIVE FOR C-189 and C-190

\*\* APPROX. STAG. PRESSURE MEASURED AT SENSOR 5

+ MEASURED AT CENTER OF MODEL

++ ASSUMED SAME AS  $T_{1A}$

• ALL VALUES WITH SUBSCRIPTS 39, 38, OR 37 ESTIMATED FROM NEARBY MEASUREMENTS

ORIGINAL PAGE IS OF POOR QUALITY

TABLE II. REFERENCE HEATING RATES USED IN WING GLOVE MODEL THERMAL ANALYSIS

A. Run 188

<u>TIME (SEC)</u>	<u>q<sub>REF 37</sub> (BTU/FT<sup>2</sup>-SEC)</u>	<u>q<sub>REF 38</sub> (BTU/FT<sup>2</sup>-SEC)</u>	<u>q<sub>REF 39</sub> (BTU/FT<sup>2</sup>-SEC)</u>
0	0.0298	0.034	0.034
20	1.78	3.88	6.4
40	2.40	5.38	8.99
80	2.27	5.055	8.42
800	2.27	5.055	8.42

ORIGINAL PAGE IS  
 OF POOR QUALITY

B. Run 189

<u>TIME (SEC)</u>	<u>q<sub>REF 37</sub> (BTU/FT<sup>2</sup>-SEC)</u>	<u>q<sub>REF 38</sub> (BTU/FT<sup>2</sup>-SEC)</u>	<u>q<sub>REF 39</sub> (BTU/FT<sup>2</sup>-SEC)</u>
0	0.02792	0.03193	0.03193
30	2.8046	6.606	10.651
45	3.0730	7.288	11.805
200	2.7530	6.475	10.446
800	2.5539	5.972	9.619

C. Run 190

<u>TIME (SEC)</u>	<u>q<sub>REF 37</sub> (BTU/FT<sup>2</sup>-SEC)</u>	<u>q<sub>REF 38</sub> (BTU/FT<sup>2</sup>-SEC)</u>	<u>q<sub>REF 39</sub> (BTU/FT<sup>2</sup>-SEC)</u>
0	0.0824	0.135	0.1576
20	2.319	6.48	8.71
60	3.344	9.65	13.09
80	3.289	9.48	12.85
115	3.457	10.01	13.58
190	3.457	10.01	13.58
270	3.752	10.94	14.87
630	3.813	11.13	15.14
800	3.937	11.52	15.68

TABLE II. REFERENCE HEATING RATES USED IN WING GLOVE MODEL THERMAL ANALYSIS  
 (CONCLUDED)

D. Run 194

<u>TIME (SEC)</u>	<u>q<sub>REF 37</sub> (BTU/FT<sup>2</sup>-SEC)</u>	<u>q<sub>REF 38</sub> (BTU/FT<sup>2</sup>-SEC)</u>	<u>q<sub>REF 39</sub> (BTU/FT<sup>2</sup>-SEC)</u>
0	0.029	0.035	0.035
60	2.35	6.20	8.80
120	3.25	8.0	12.60
200	3.49	9.50	13.60
800	3.49	9.50	13.60

ORIGINAL PAGE  
 OF POOR QUALITY

E. Run 195

<u>TIME (SEC)</u>	<u>q<sub>REF 37</sub> (BTU/FT<sup>2</sup>-SEC)</u>	<u>q<sub>REF 38</sub> (BTU/FT<sup>2</sup>-SEC)</u>	<u>q<sub>REF 39</sub> (BTU/FT<sup>2</sup>-SEC)</u>
0	0.029	0.0344	0.0376
10	1.07	2.40	3.58
20	2.46	5.97	9.22
40	3.53	8.81	13.76
80	3.40	8.49	13.25
530	3.07	7.58	11.78
1000	3.07	7.58	11.78

FIG. 1 SURFACE PRESSURES ON WING GLOVE MODEL FOR FIVE CASES INVESTIGATED

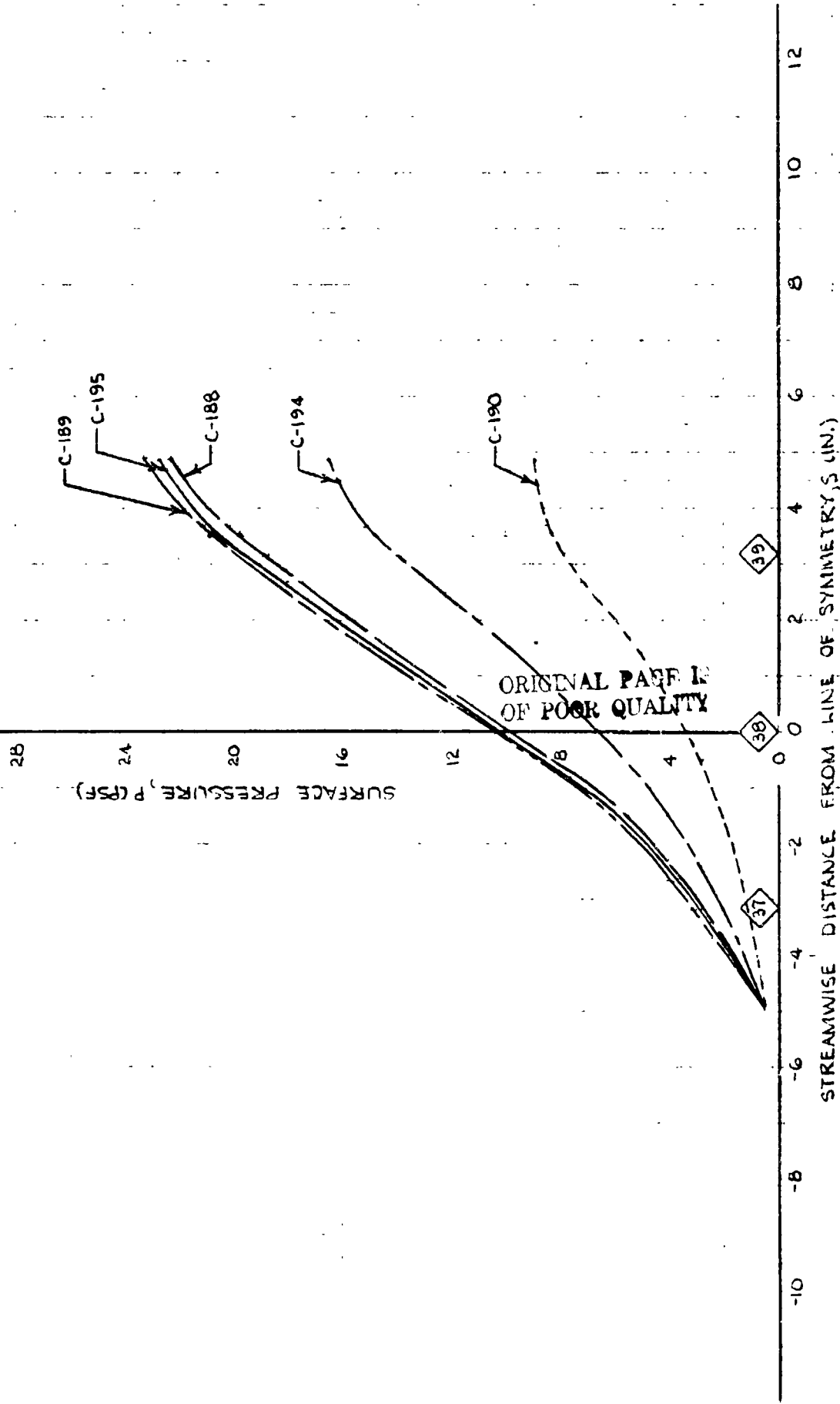
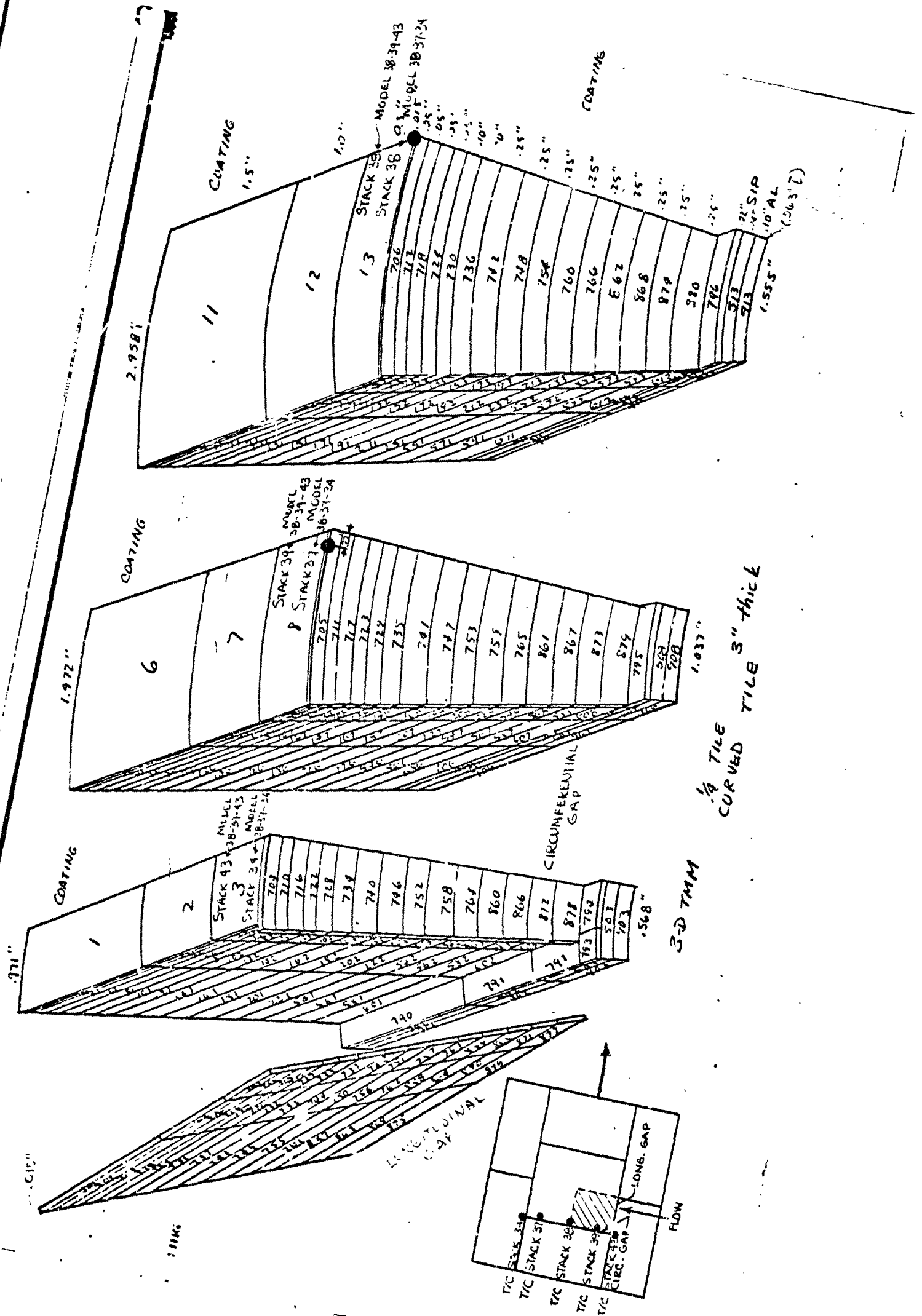


FIG. 2. SKETCH OF 3-D CURVED TILE MODEL



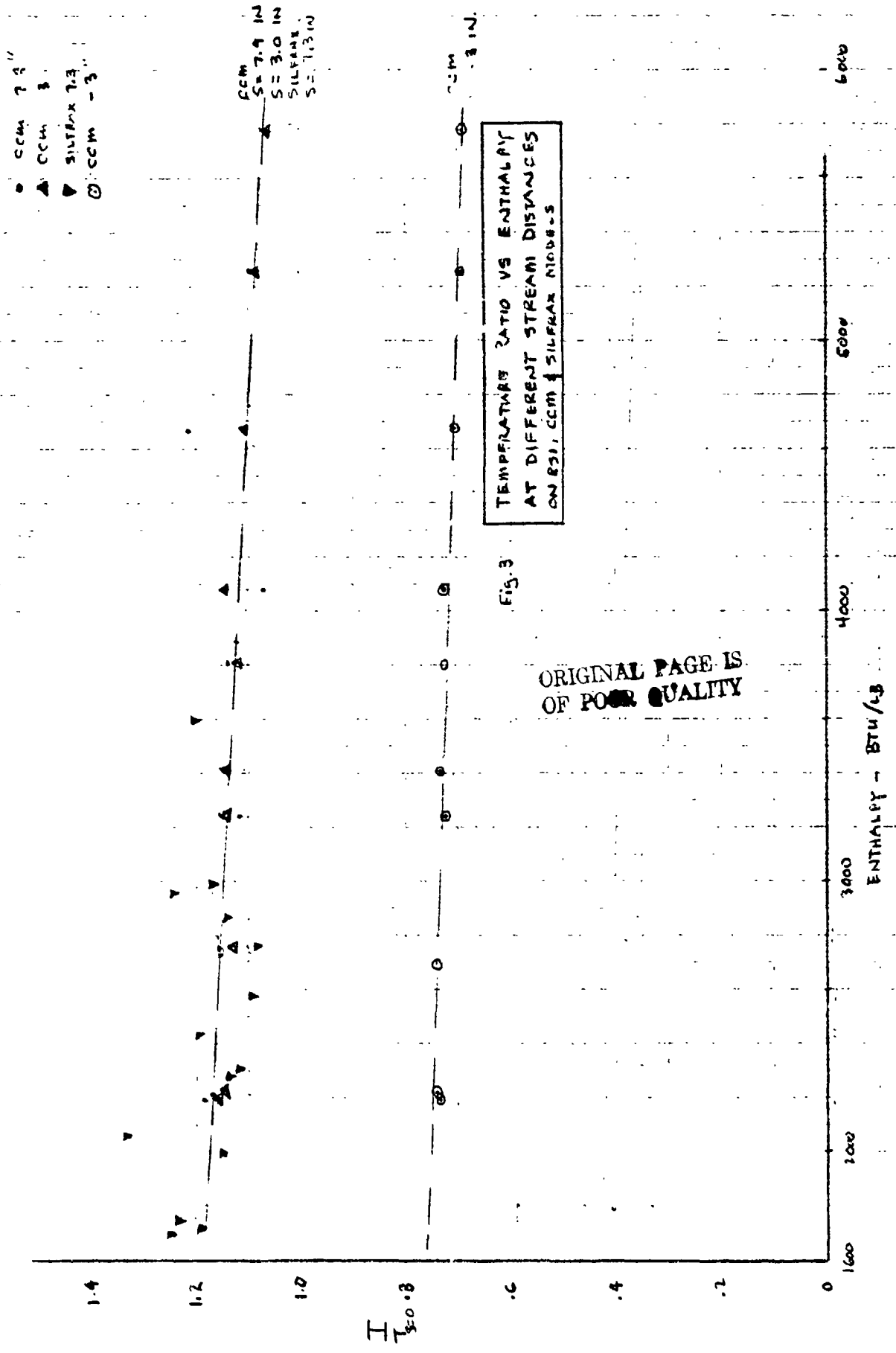
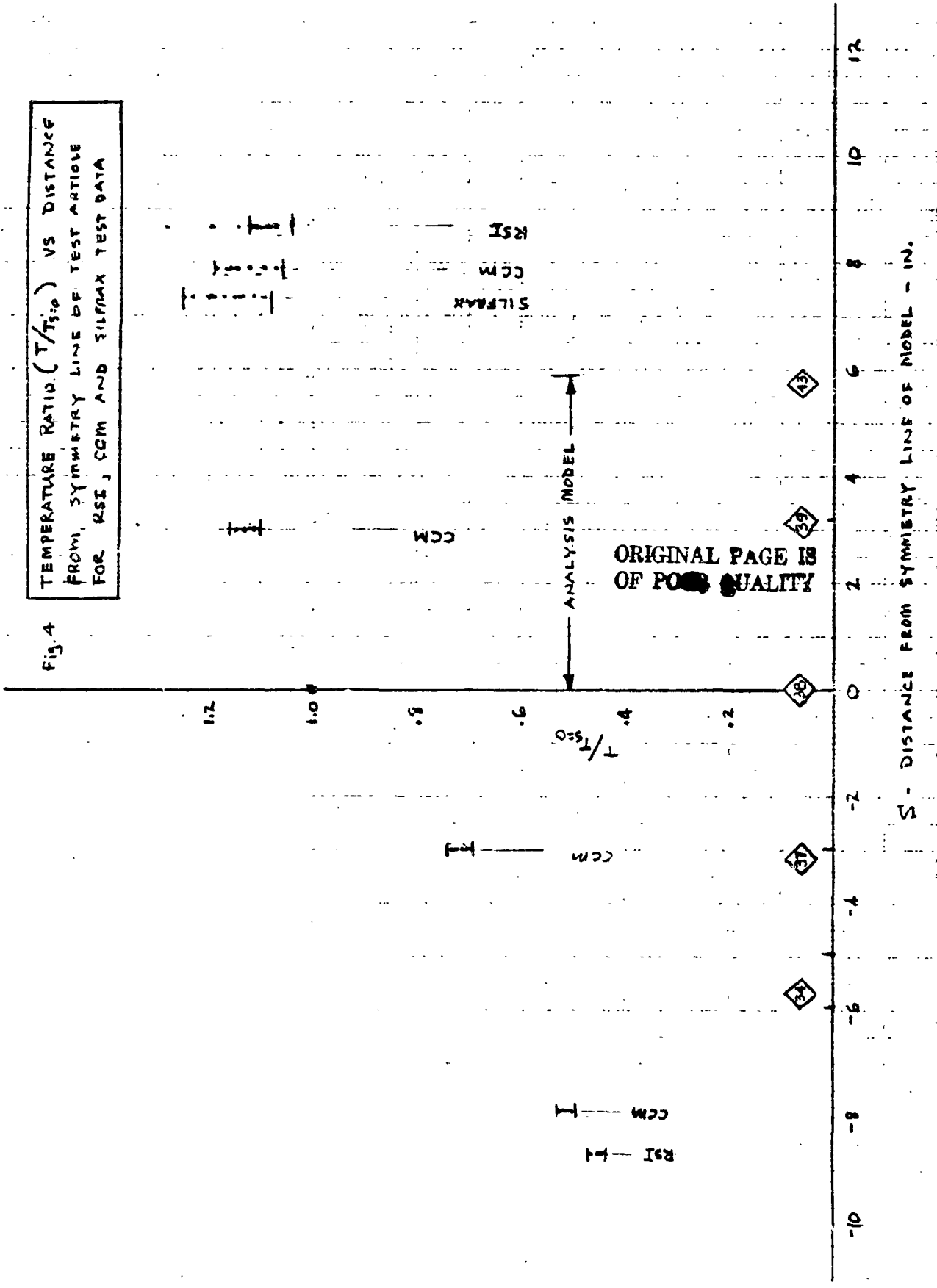


Fig. 4  
 TEMPERATURE RATIO ( $T/T_{s=0}$ ) VS DISTANCE  
 FROM SYMMETRY LINE OF TEST ARTICLE  
 FOR RSI, CCM AND SILFRAX TEST DATA



S - DISTANCE FROM SYMMETRY LINE OF MODEL - IN.

Fig. 5

GAP IN-DEPTH TEMPERATURE PROFILE AT  
DISCRETE TIME FRAMES FOR T/C STACK # 39  
FOR  $\alpha = 45^\circ$ ,  $\beta = 0^\circ$ ;  $\dot{m} = 1.032$  LB/SEC;  $I = 1292$  AMPS (C-188)

NOTE: BEST-FIT CORRELATION

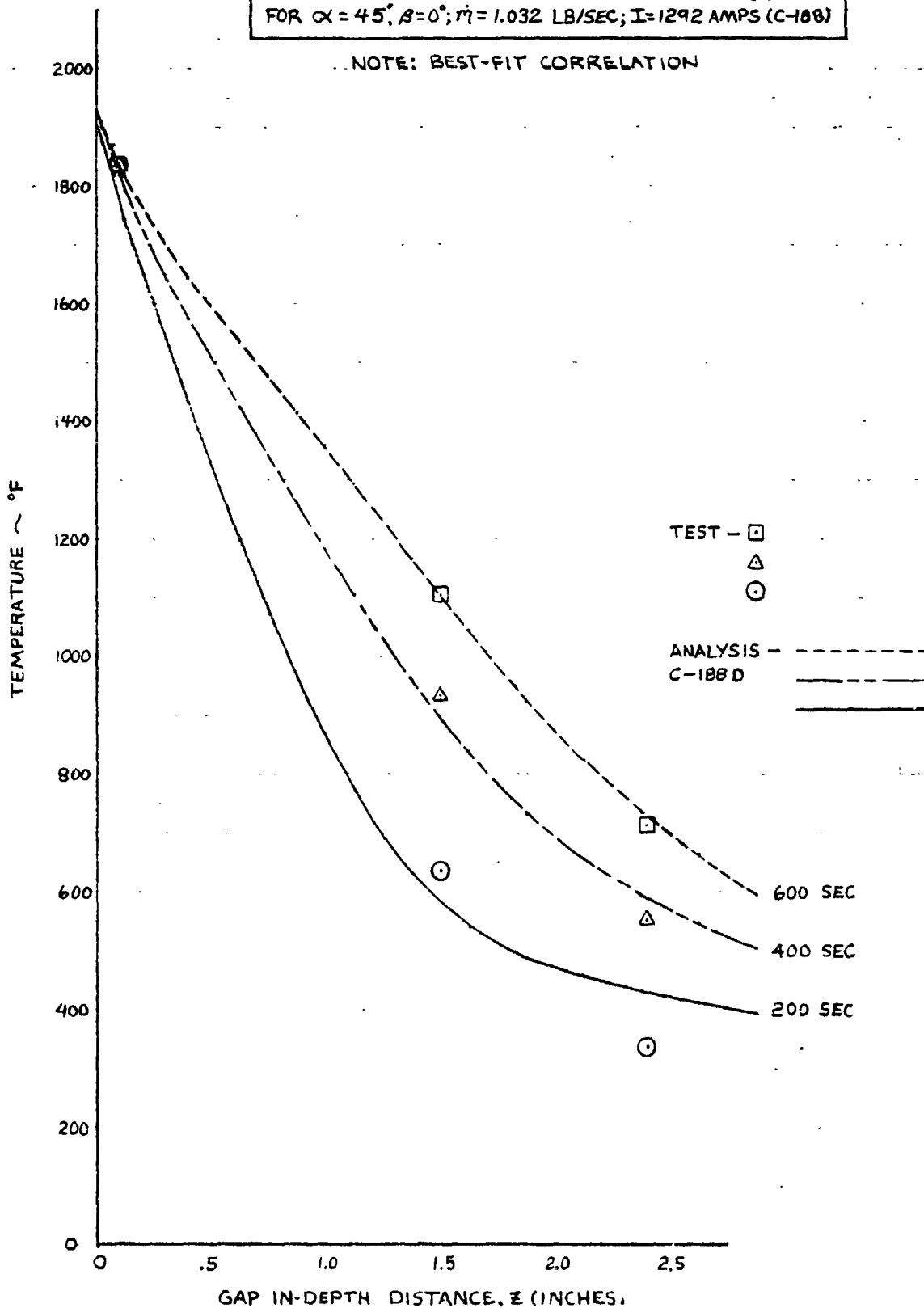
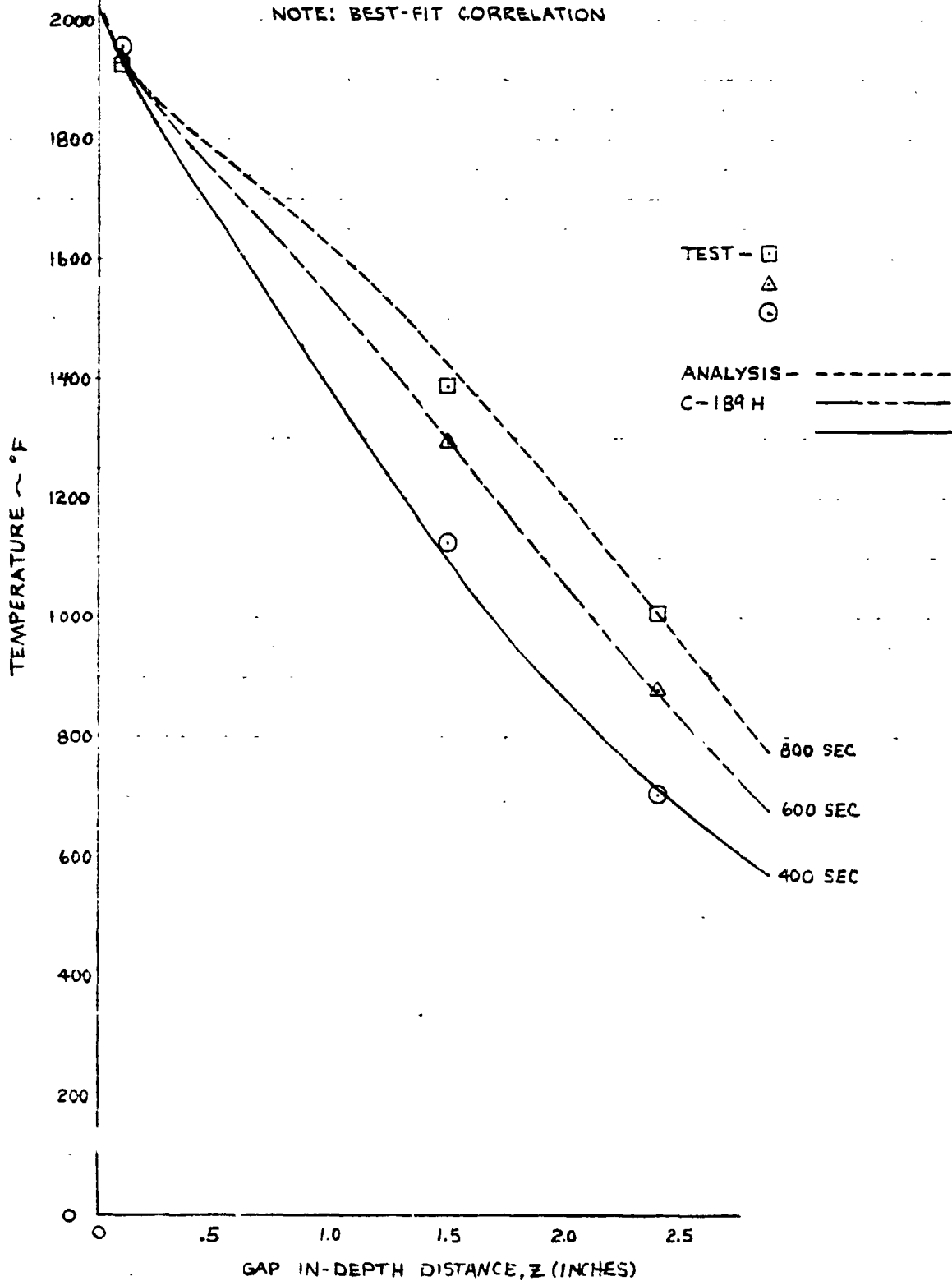


Fig. 6 GAP IN-DEPTH TEMPERATURE PROFILE AT DISCRETE TIME FRAMES FOR T/C STACK #39 FOR  $\alpha = 45^\circ$ ,  $\beta = 0^\circ$ ;  $\dot{m} = 960$  LB/SEC;  $I = 1622$  AMPS (C-189)



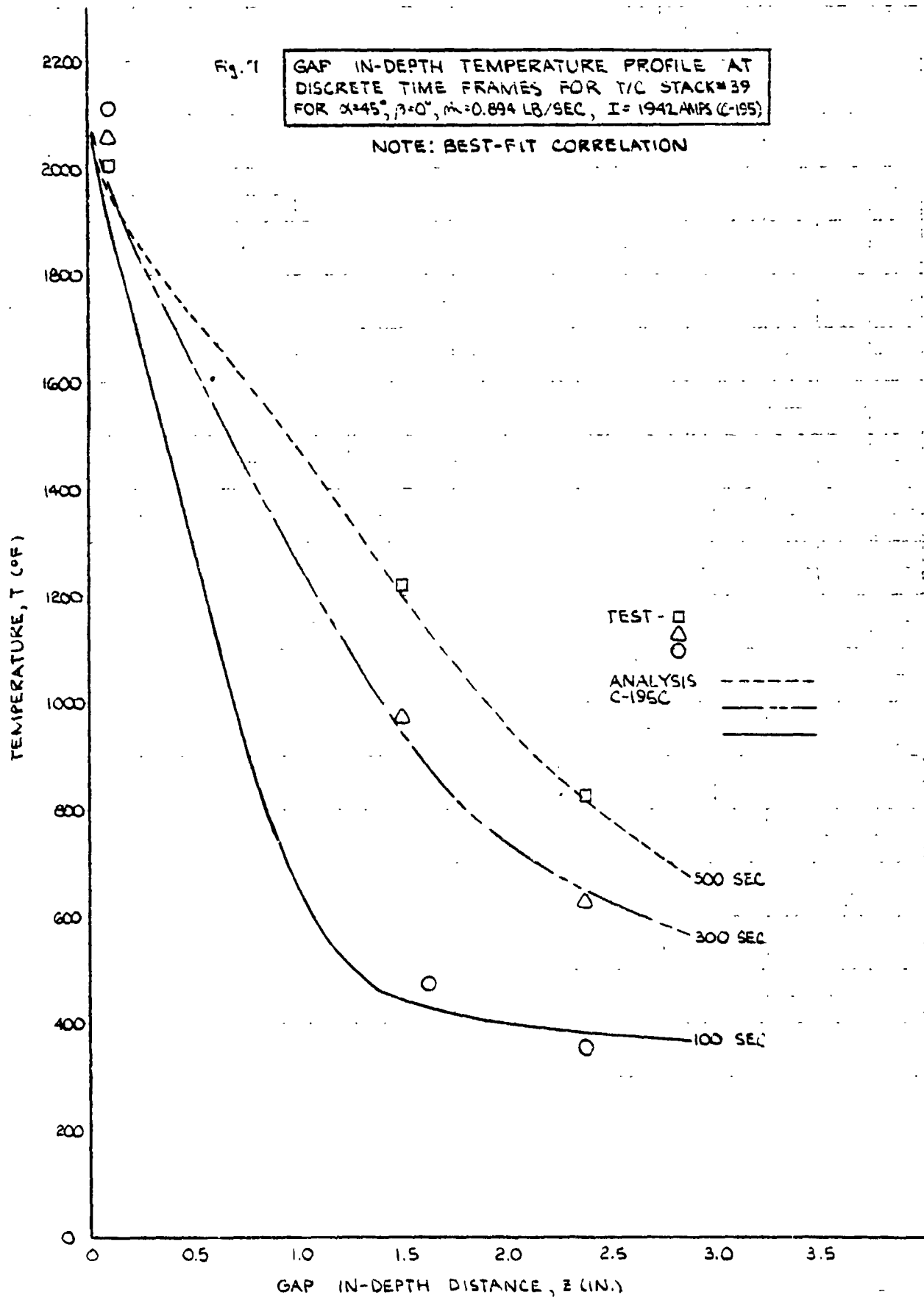


Fig. 8

GAP IN-DEPTH TEMPERATURE PROFILE AT DISCRETE TIME FRAMES FOR T/C STACK #39 FOR  $\alpha = 45^\circ$ ;  $\beta = 0^\circ$ ;  $\dot{m} = .559$  LB/SEC;  $I = 1942$  AMPS (C-194)

NOTE: BEST-FIT CORRELATION

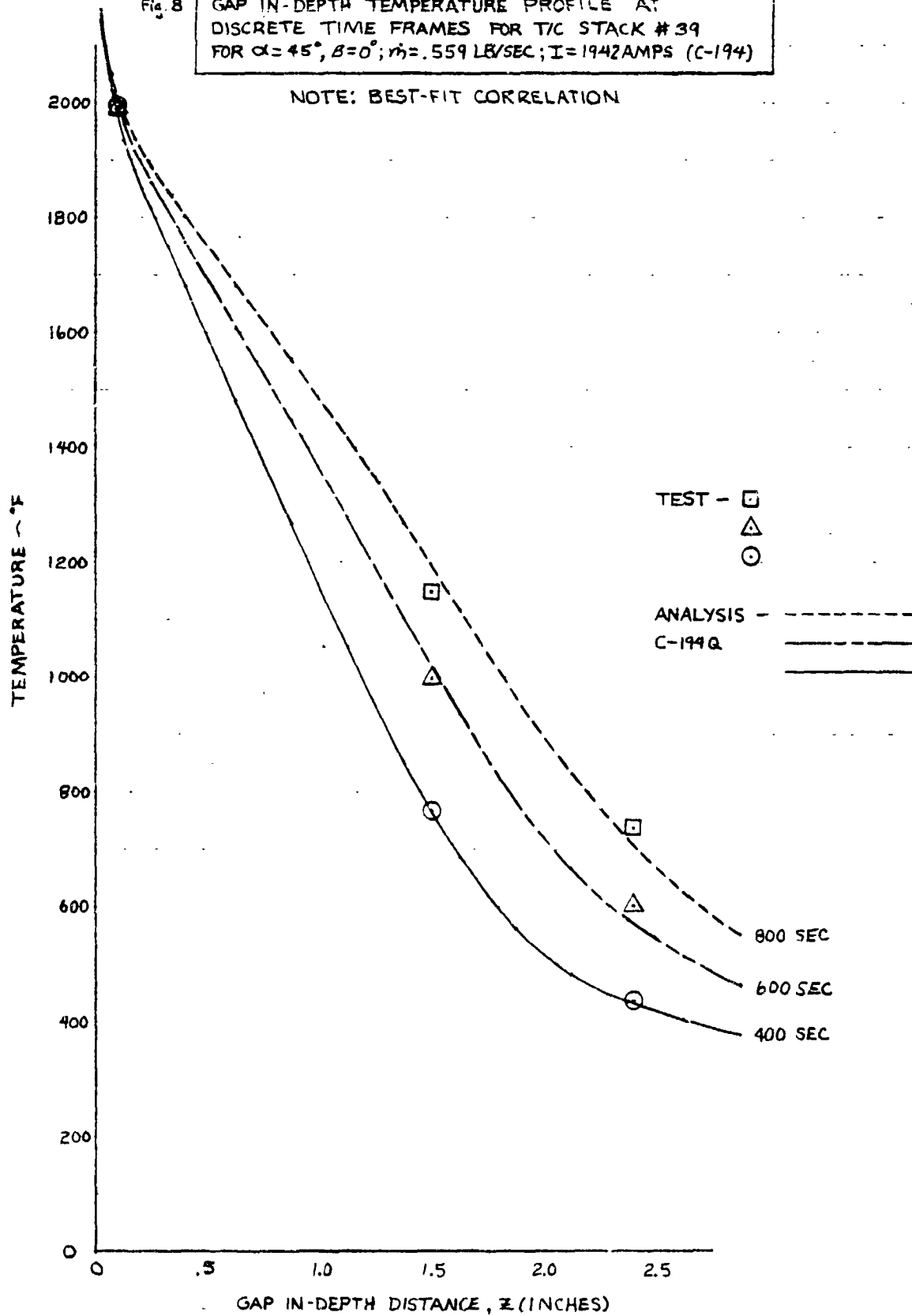


Fig. 9

GAP IN-DEPTH TEMPERATURE PROFILE AT DISCRETE TIME FRAMES FOR T/C STACK #39 FOR  $\alpha=75^\circ, \beta=0^\circ; \dot{m}=0.258 \text{ LB/SEC}; I=1491 \text{ AMPS (C-190)}$

NOTE: BEST-FIT CORRELATION

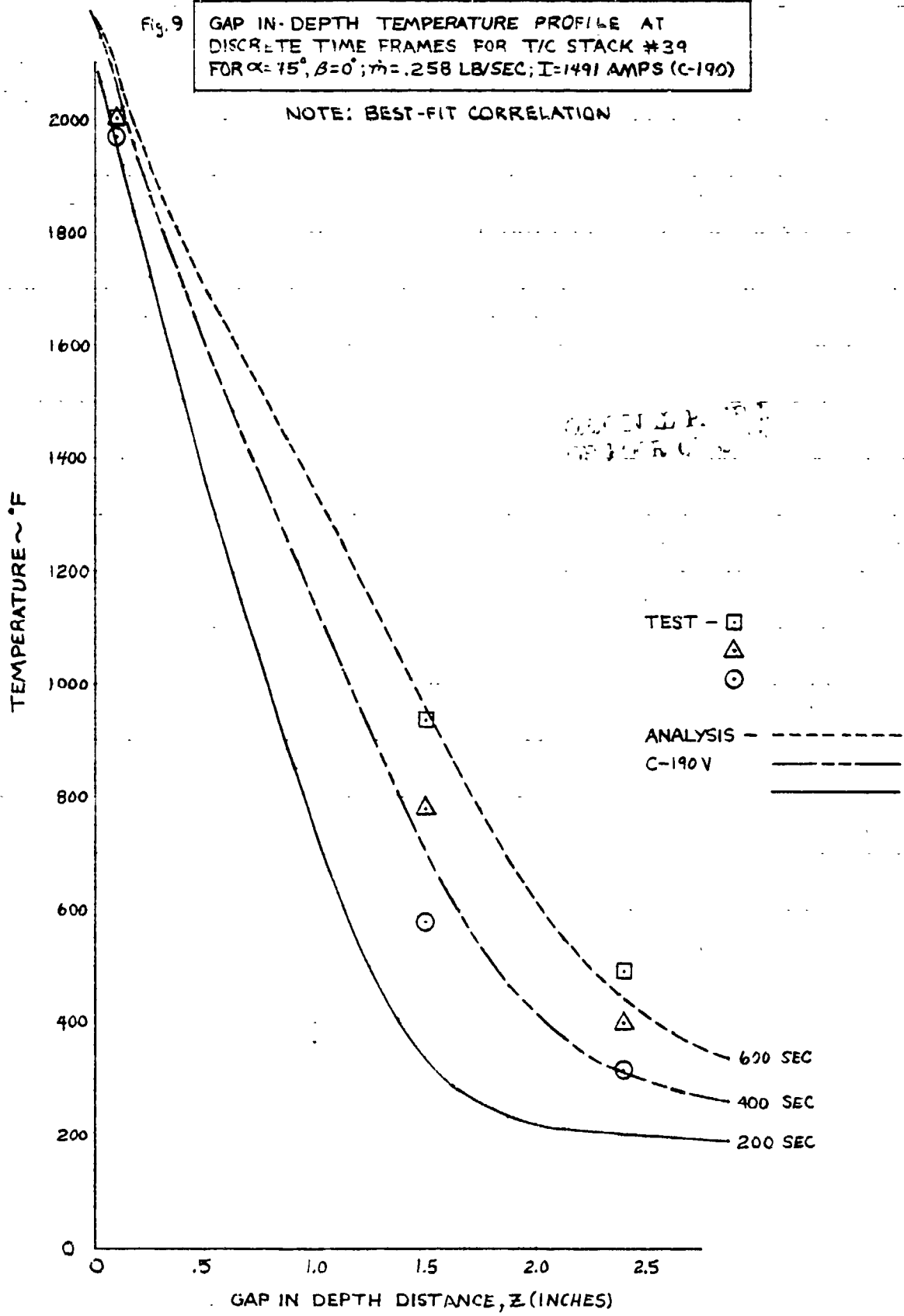


Fig. 10

GAP IN-DEPTH TEMPERATURE PROFILE AT  
DISCRETE TIME FRAMES FOR T/C STACK #38  
FOR  $\alpha=45^\circ$ ,  $\beta=0^\circ$ ;  $\dot{m}=1.032$  LB/SEC;  $I=1292$  AMPS (C-188)

NOTE: BEST-FIT CORRELATION

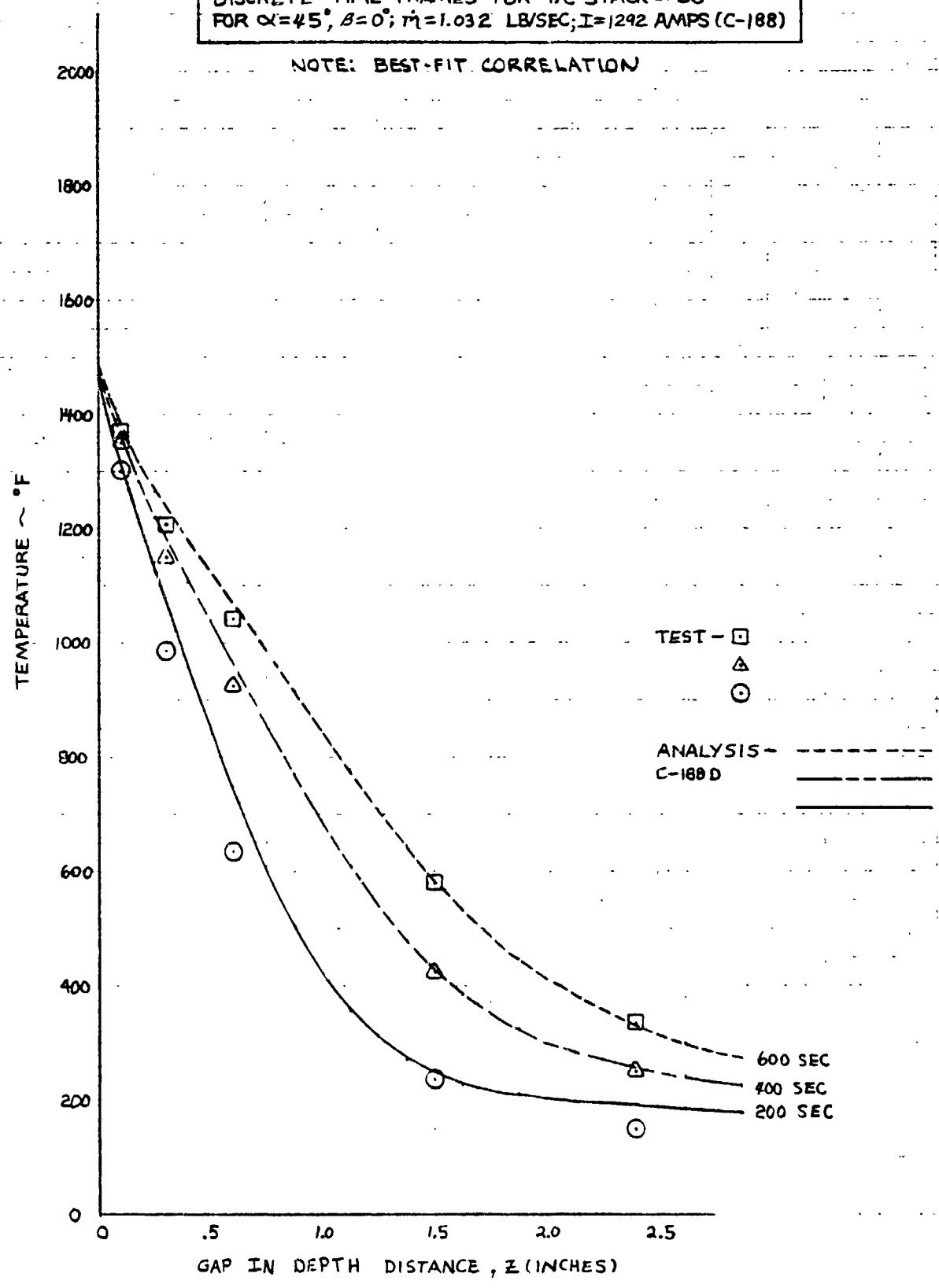


Fig. 11

GAP IN-DEPTH TEMPERATURE PROFILE AT  
DISCRETE TIME FRAMES FOR T/C STACK #38  
FOR  $\alpha = 45^\circ$ ,  $\beta = 0^\circ$ ;  $\dot{m} = .760$  LB/SEC;  $I = 1622$  AMPS (C-189)

NOTE: BEST-FIT CORRELATION

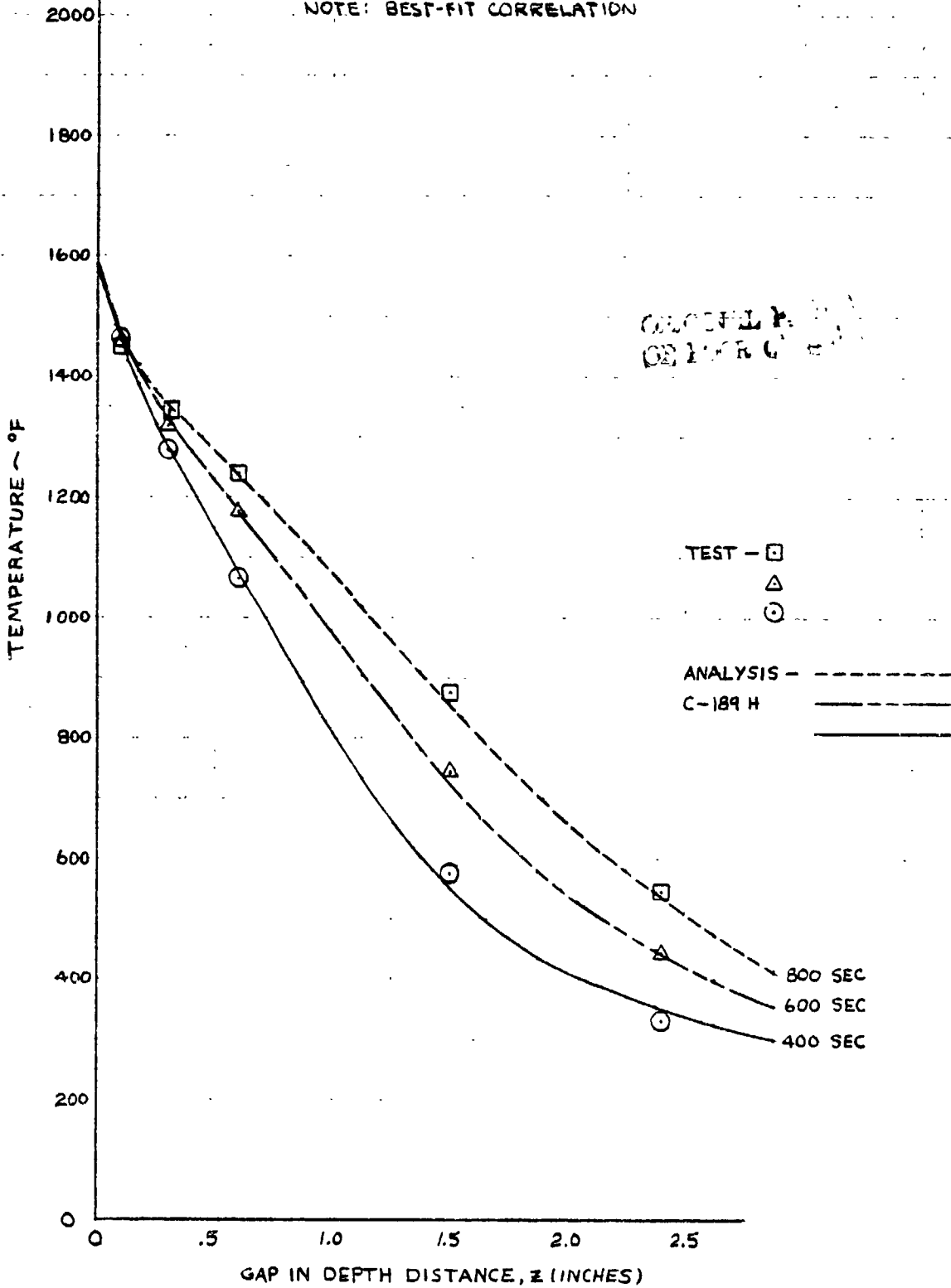


Fig. 12 GAP IN-DEPTH TEMPERATURE PROFILE AT DISCRETE TIME FRAMES FOR T/C STACK # 3B FOR  $\alpha=45^\circ$ ,  $\beta=0^\circ$ ,  $m=0.894$  LB/SEC,  $I=1942$  AMPS (C-195)

NOTE: BEST-FIT CORRELATION

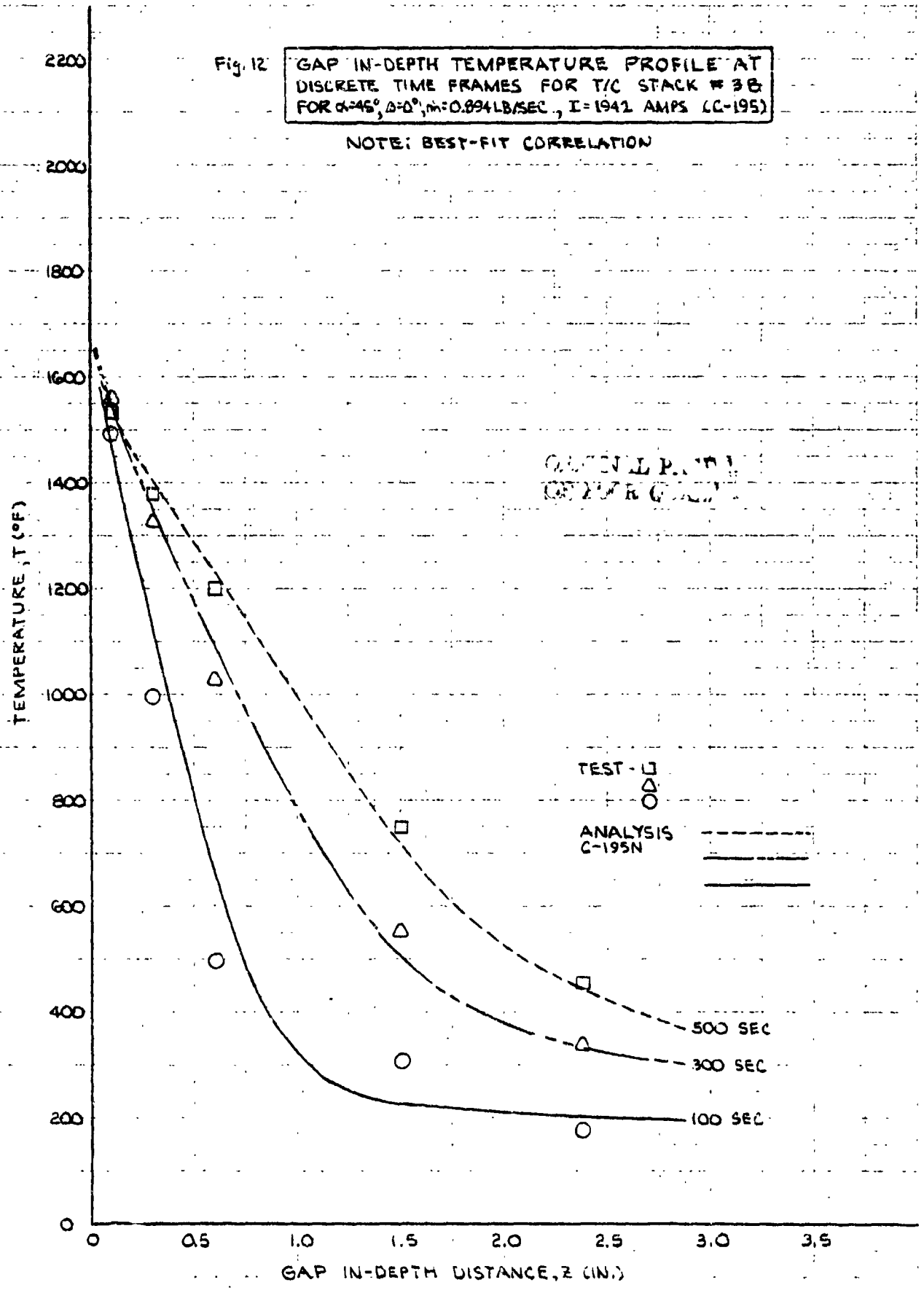


Fig. 13 GAP IN-DEPTH TEMPERATURE PROFILE AT DISCRETE TIME FRAMES FOR T/C STACK # 38 FOR  $\alpha=45^\circ, \beta=0^\circ; \dot{m}=.559 \text{ LB/SEC}; I=1942 \text{ AMPS (C-194)}$

NOTE: BEST-FIT CORRELATION.

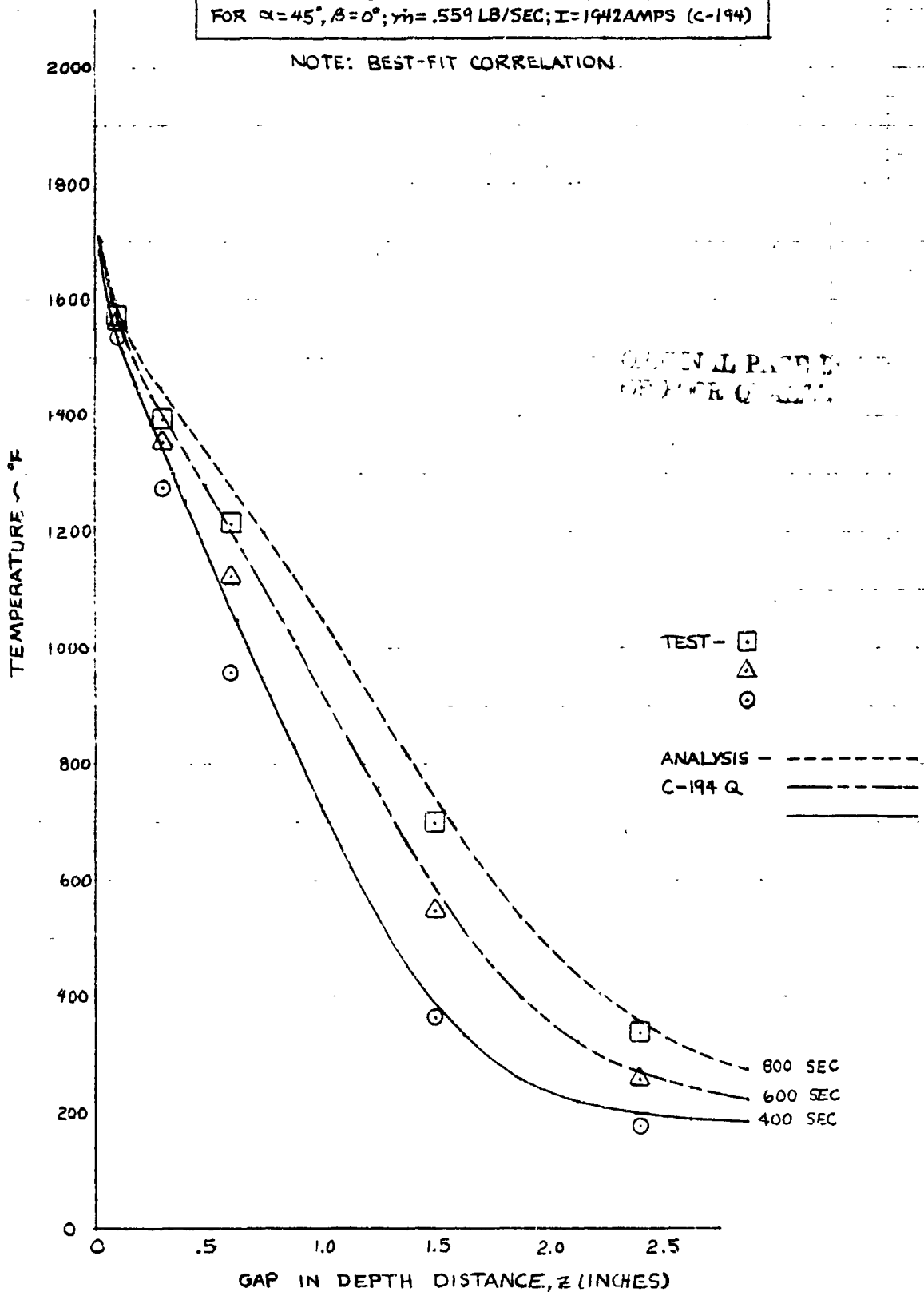


Fig. 14

GAP IN-DEPTH TEMPERATURE PROFILE AT  
DISCRETE TIME FRAMES FOR T/C STACK #36  
FOR  $\alpha=45^\circ, \beta=0^\circ; \dot{m}=0.258 \text{ LB/SEC}; I=1491 \text{ AMPS (C-190)}$

- "ZERO  $\Delta P$ " (B/L)  $\dot{q}/\dot{q}_{REF}$

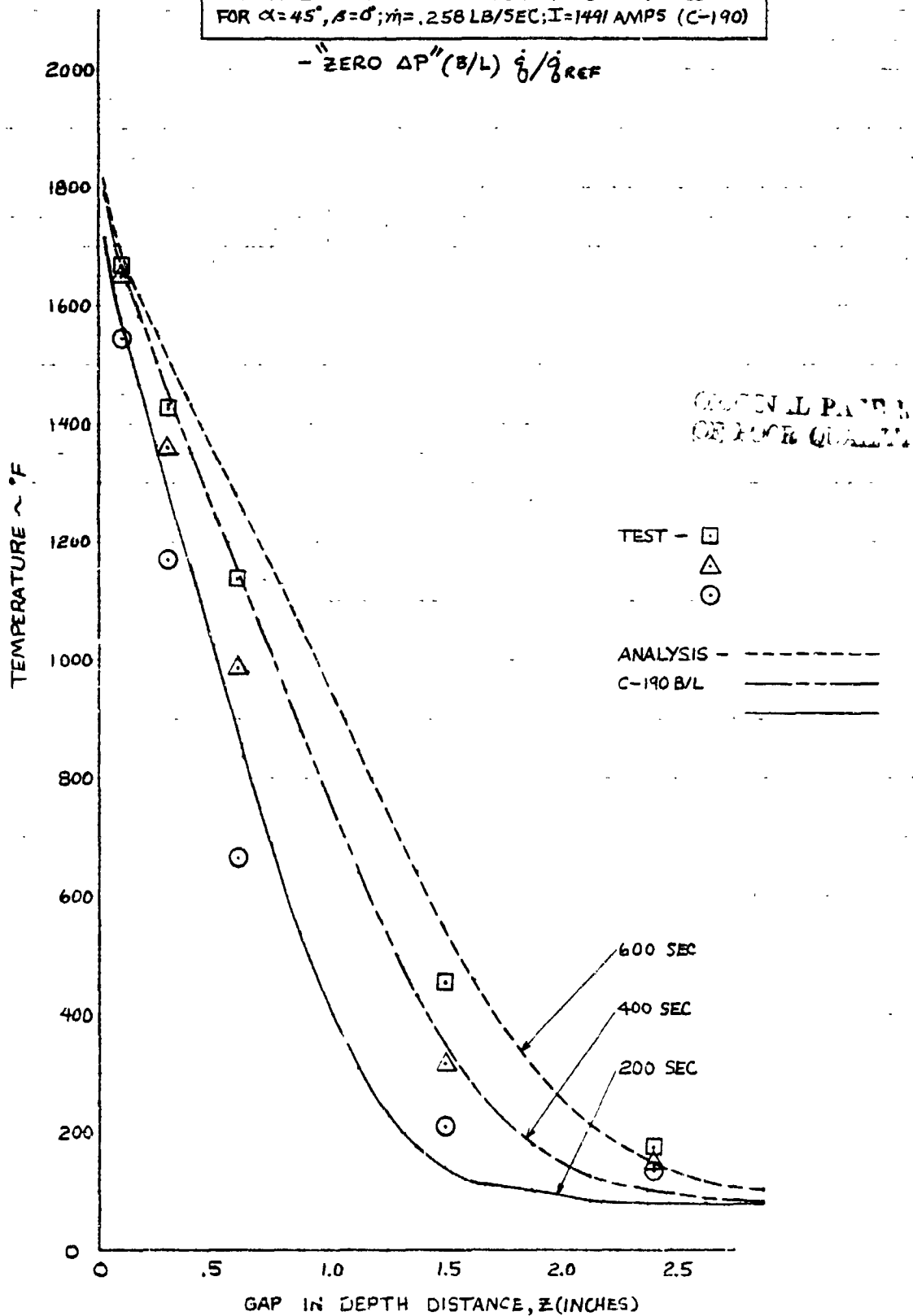


Fig. 15

COMPARISON OF GAP IN-DEPTH TEMPERATURES WITH  
BASELINE PREDICTIONS FOR T/C STACK #37 FOR  
 $\alpha=45^\circ$ ;  $\beta=0^\circ$ ;  $\dot{m}=1.0$  LB/SEC;  $I=1292$  AMPS (C-188)

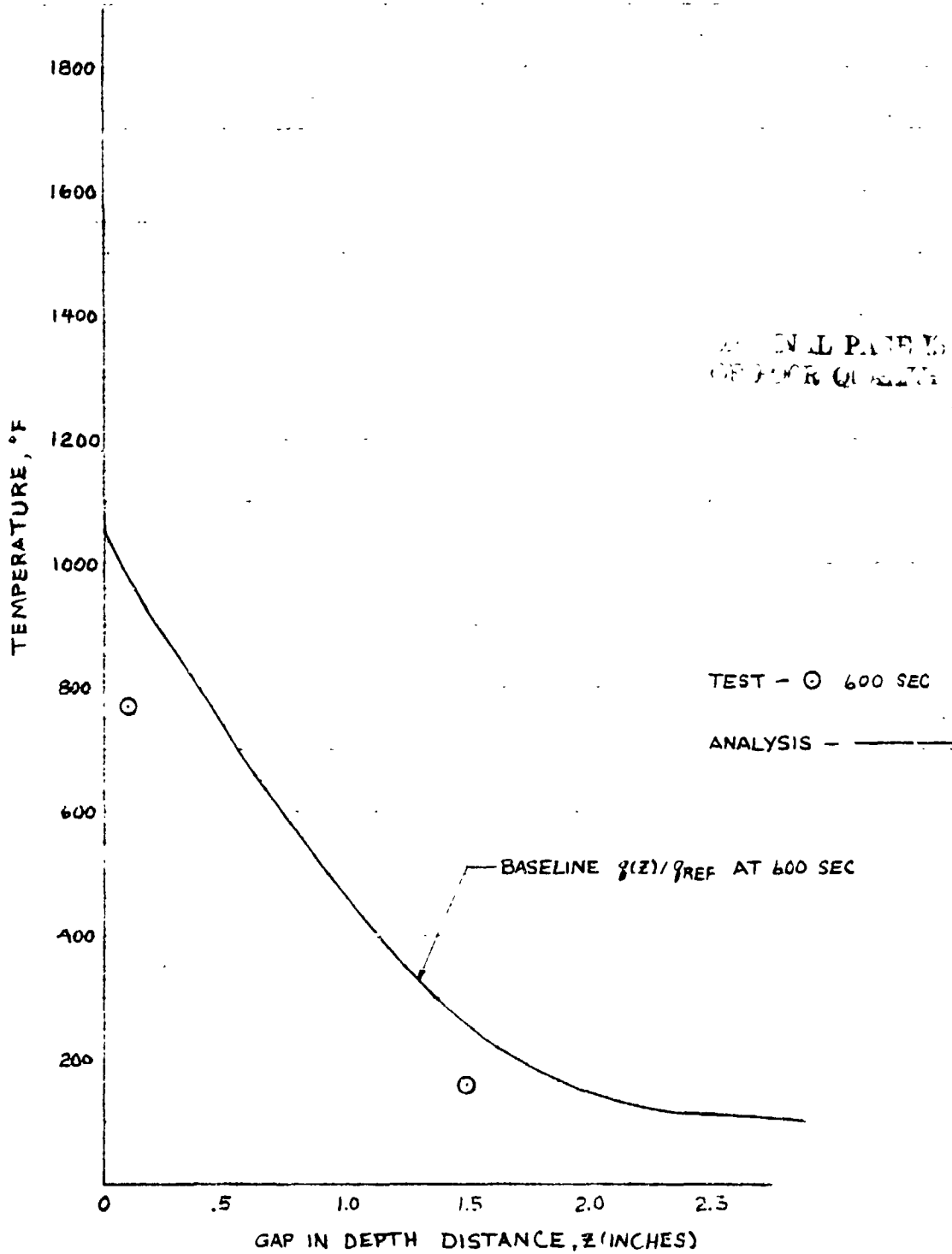


Fig. 16

COMPARISON OF GAP IN-DEPTH TEMPERATURES WITH  
BASELINE PREDICTIONS FOR T/C STACK #37 FOR  
 $\alpha = 45^\circ$ ,  $\beta = 0^\circ$ ;  $\dot{m} = 0.96$  LB/SEC;  $I = 1622$  AMPS (C-189)

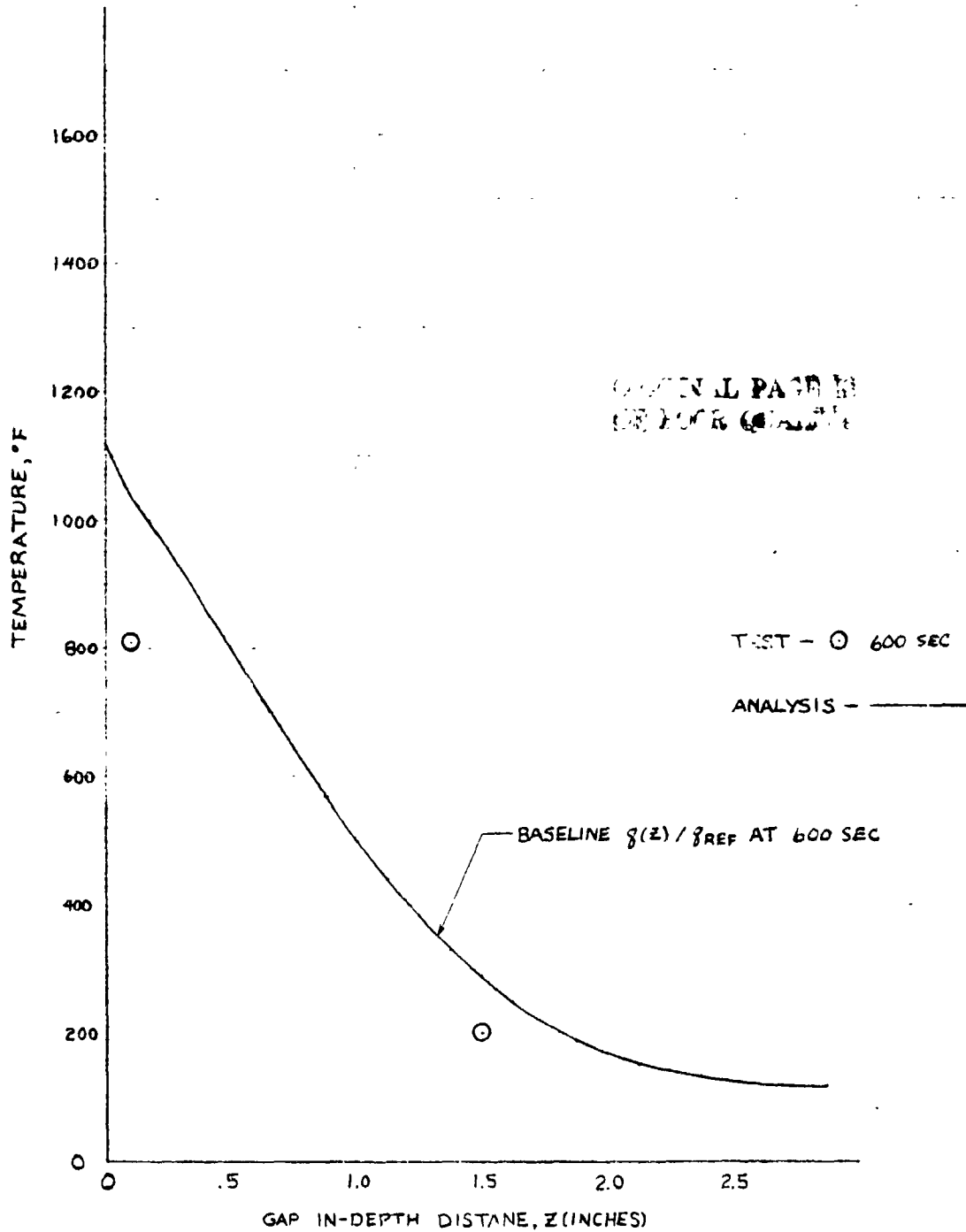




Fig 18

COMPARISON OF GAP IN-DEPTH TEMPERATURES WITH  
BASELINE PREDICTIONS FOR T/C STACK # 37 FOR  
 $\alpha = 45^\circ$ ,  $\beta = 0^\circ$ ;  $\dot{m} = 0.559$  LB/SEC;  $I = 1942$  AMPS (C-194)

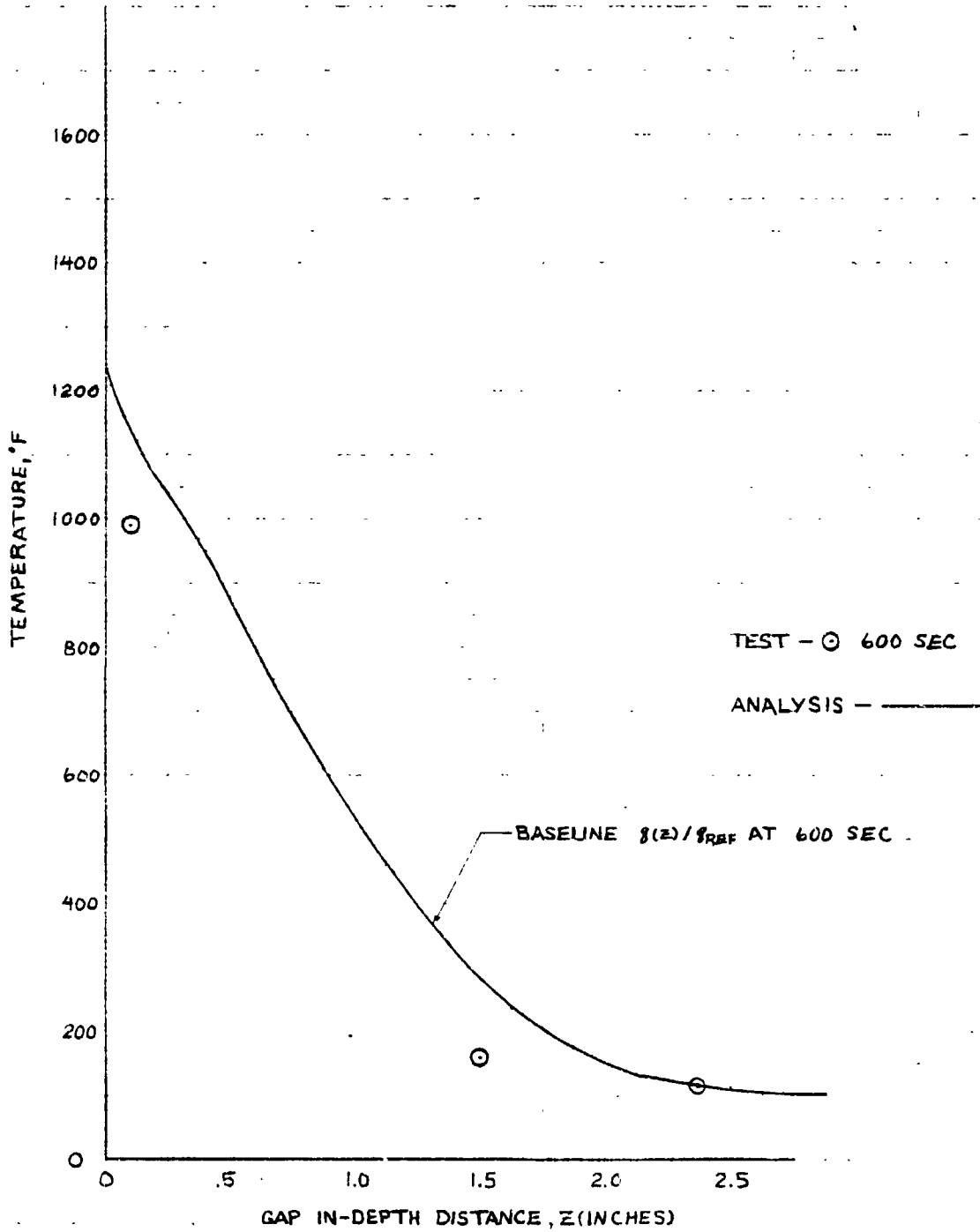


Fig. 19

COMPARISON OF GAP IN-DEPTH TEMPERATURES WITH  
BASELINE PREDICTIONS FOR T/C STACK #37 FOR  
 $\alpha = 45^\circ$ ,  $\beta = 0^\circ$ ;  $\dot{m} = 0.258$  LB/SEC;  $I = 1491$  AMPS (C-190)

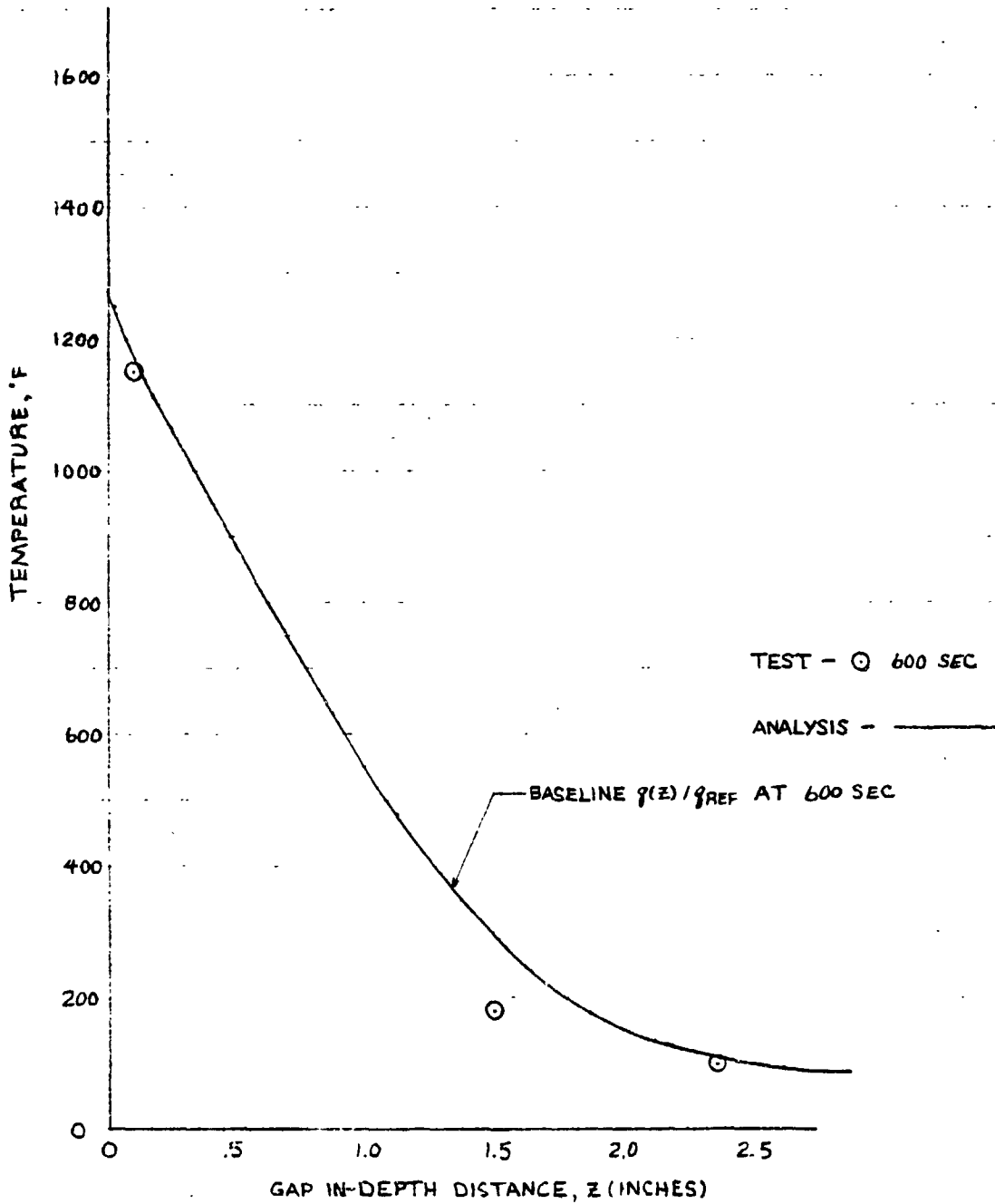
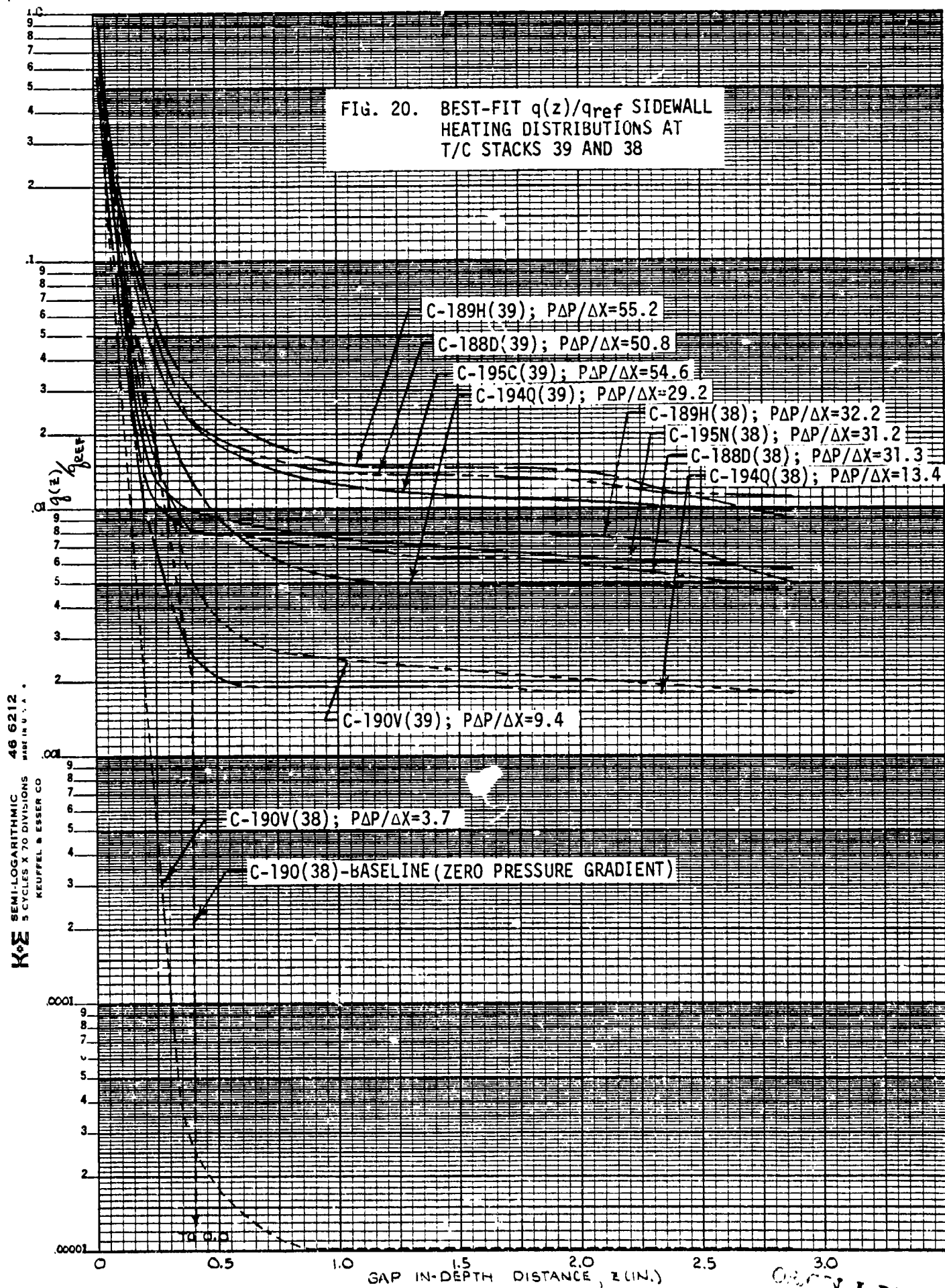


FIG. 20. BEST-FIT  $q(z)/q_{ref}$  SIDEWALL HEATING DISTRIBUTIONS AT T/C STACKS 39 AND 38



K&E SEMI-LOGARITHMIC 46 6212  
 5 CYCLES X 70 DIVISIONS  
 KEUFFEL & ESSER CO. MADE IN U.S.A.

ORIGINAL PAGE IS OF LOWER QUALITY

FIG. 21.  $q(z)/q_{ref}$  VS  $P(\Delta_i/\Delta X)$  AT VARIOUS GAP DEPTHS FOR T/C STACK 39 USING BEST-FIT CORRELATION

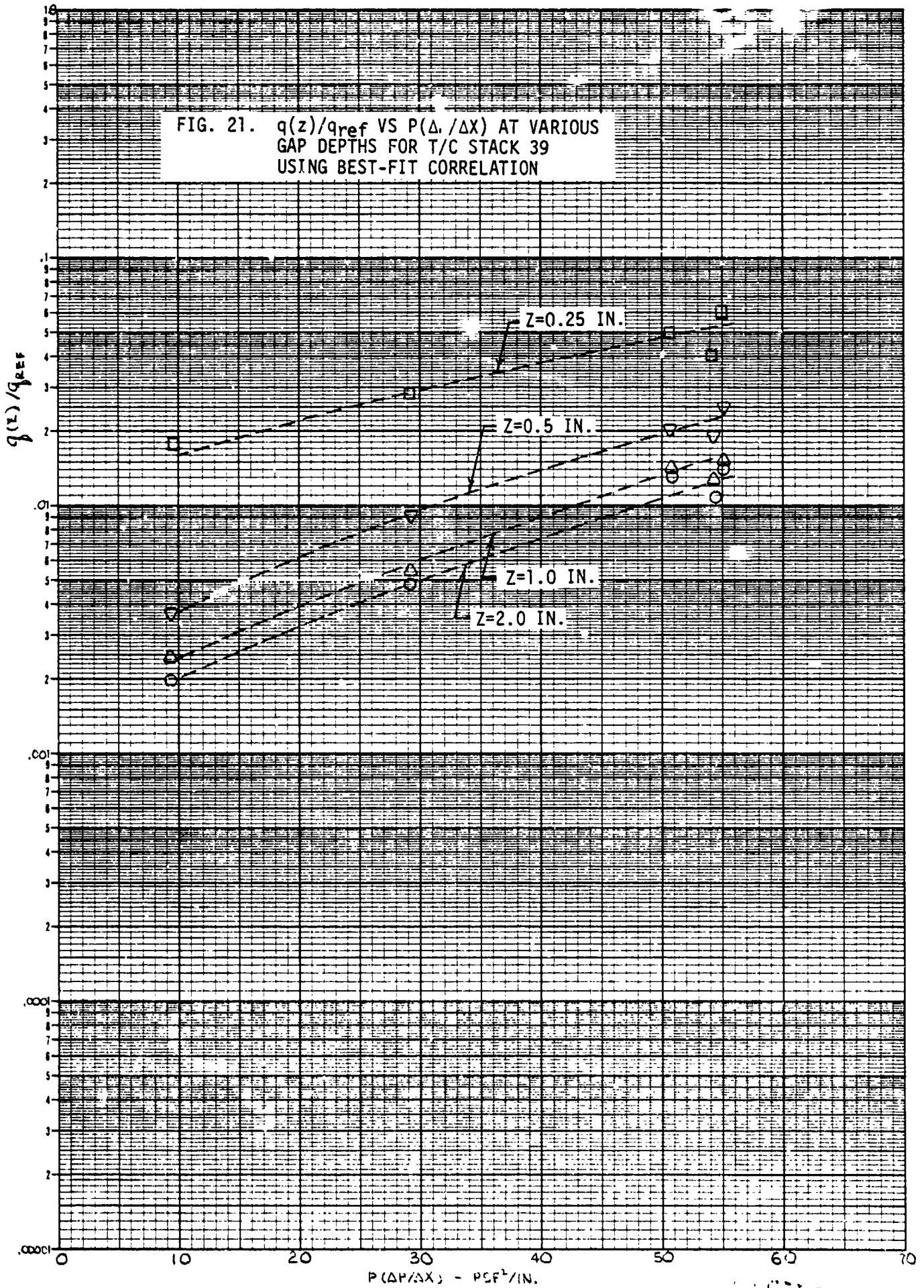
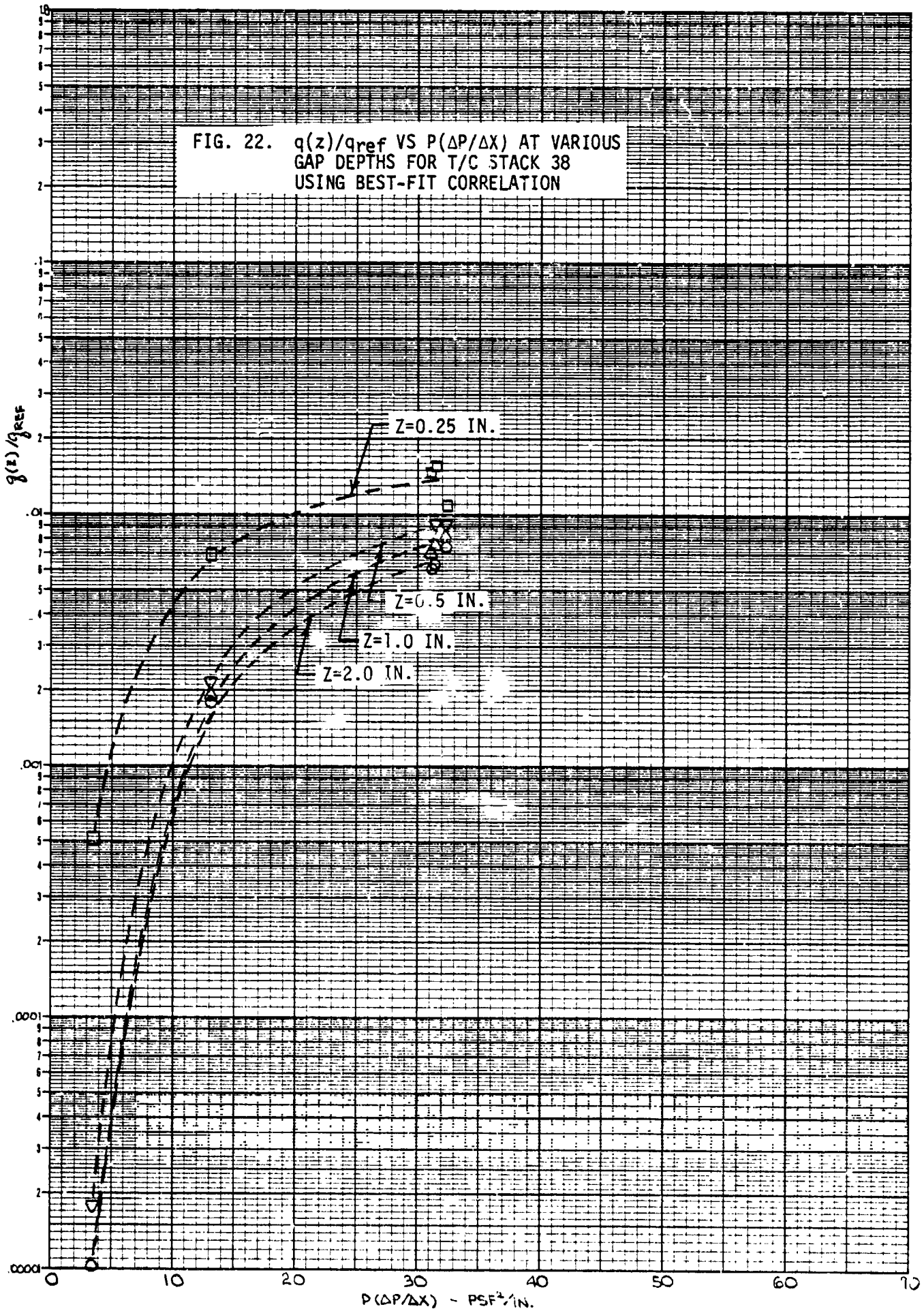
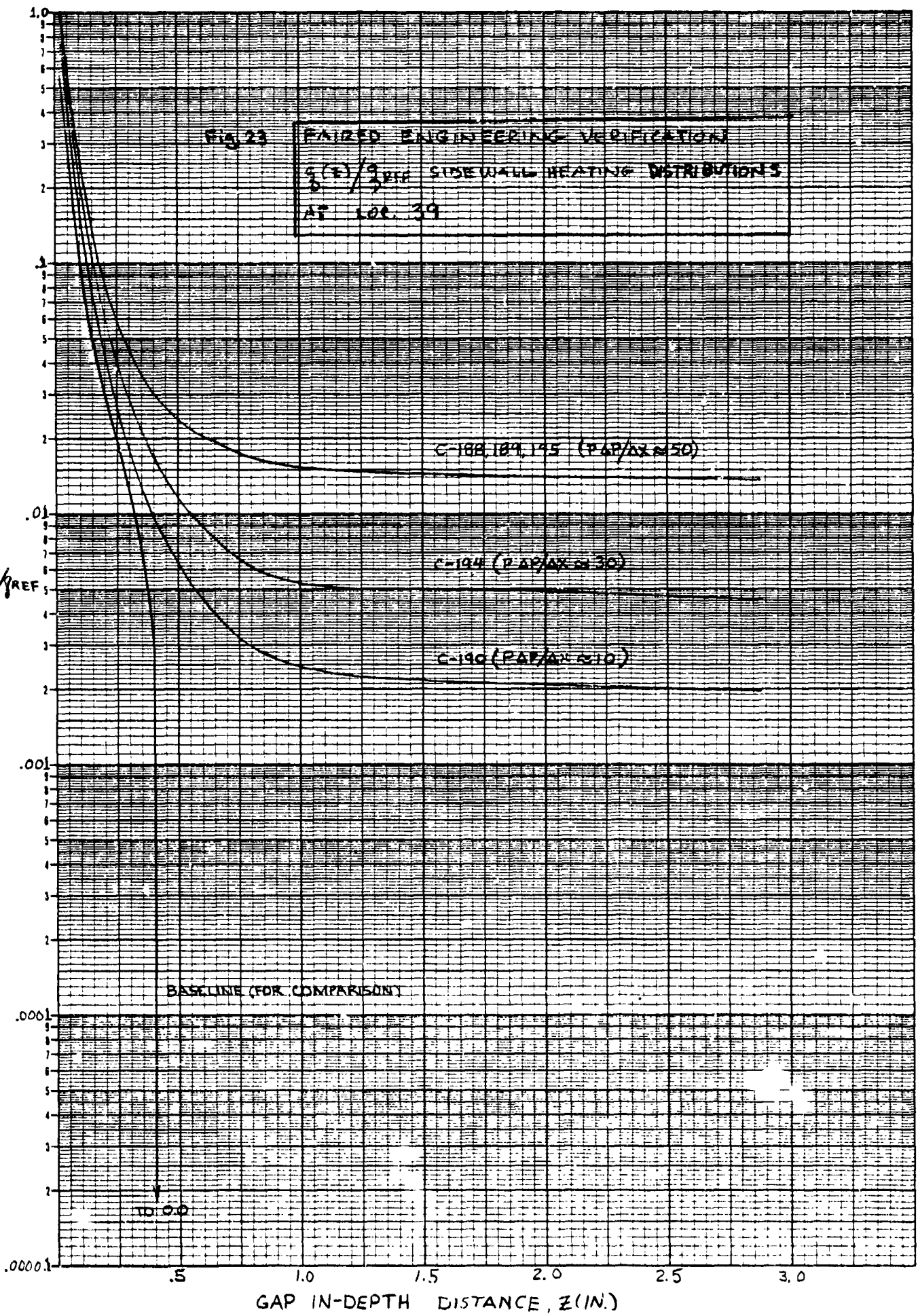


FIG. 22.  $q(z)/q_{ref}$  VS  $P(\Delta P/\Delta X)$  AT VARIOUS GAP DEPTHS FOR T/C STACK 38 USING BEST-FIT CORRELATION



GRAPHIC CONTROLS CORPORATION  
BUFFALO, N.Y.

FIG. 23 FAIRED ENGINEERING VERIFICATION  
 $\frac{q(z)}{q_{REF}}$  SIDEWALL HEATING DISTRIBUTIONS  
AT LOC. 39



ORIGINAL PHOTO COPY

SEMI LOGARITHMIC 5 CYCLES X 70 DIVISIONS AD BASE -61

GRAPHIC PAPERS GRAPHIC CONTROLS CORPORATION Buffalo, New York  
Patented in U. S. A.

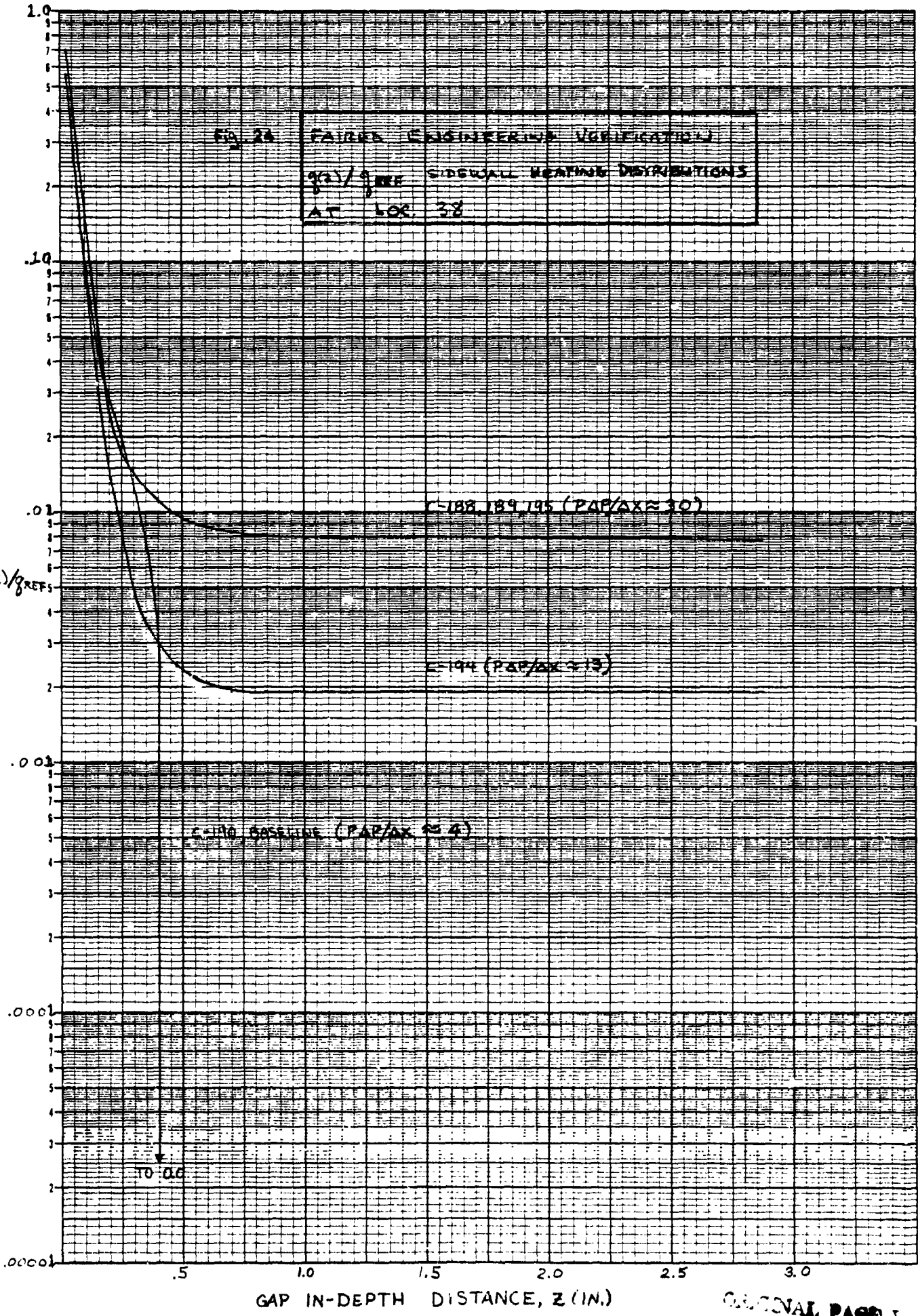


FIG. 28 FAIRBAIRN ENGINEERING VERIFICATION  
 $g(z)/g_{REF}$  LATERAL HEATING DISTRIBUTIONS  
AT LOC. 38

C=188, 189, 195 (PAR/AX ≈ 30)

C=194 (PAR/AX ≈ 15)

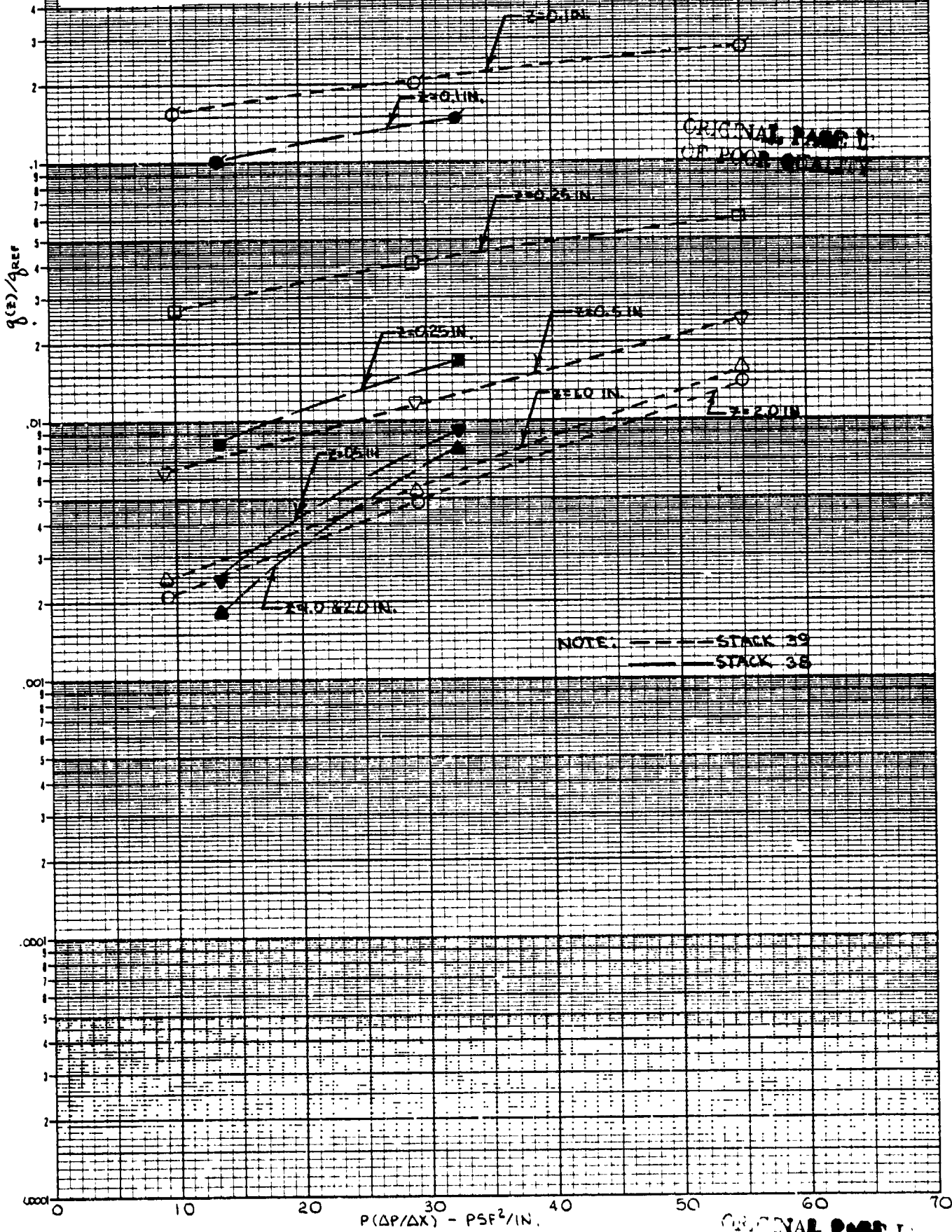
C=190 BASELINE (PAR/AX ≈ 4)

TO 0.0

GAP IN-DEPTH DISTANCE, Z (IN.)

ORIGINAL PAGE IS  
OF POOR QUALITY

FIG. 25.  $q(z)/q_{ref}$  VS  $P(\Delta P/\Delta X)$  AT VARIOUS GAP DEPTHS FOR T/C STACKS 38 & 39 USING ENGINEERING VERIFICATION CORRELATION



GRAPHIC CORPORATION Buffalo, New York  
 5 CIRCLES X 75 DIVISIONS AB-8845-GT  
 SEMI-LOGARITHMIC

ORIGINAL PAPER OF POOR QUALITY

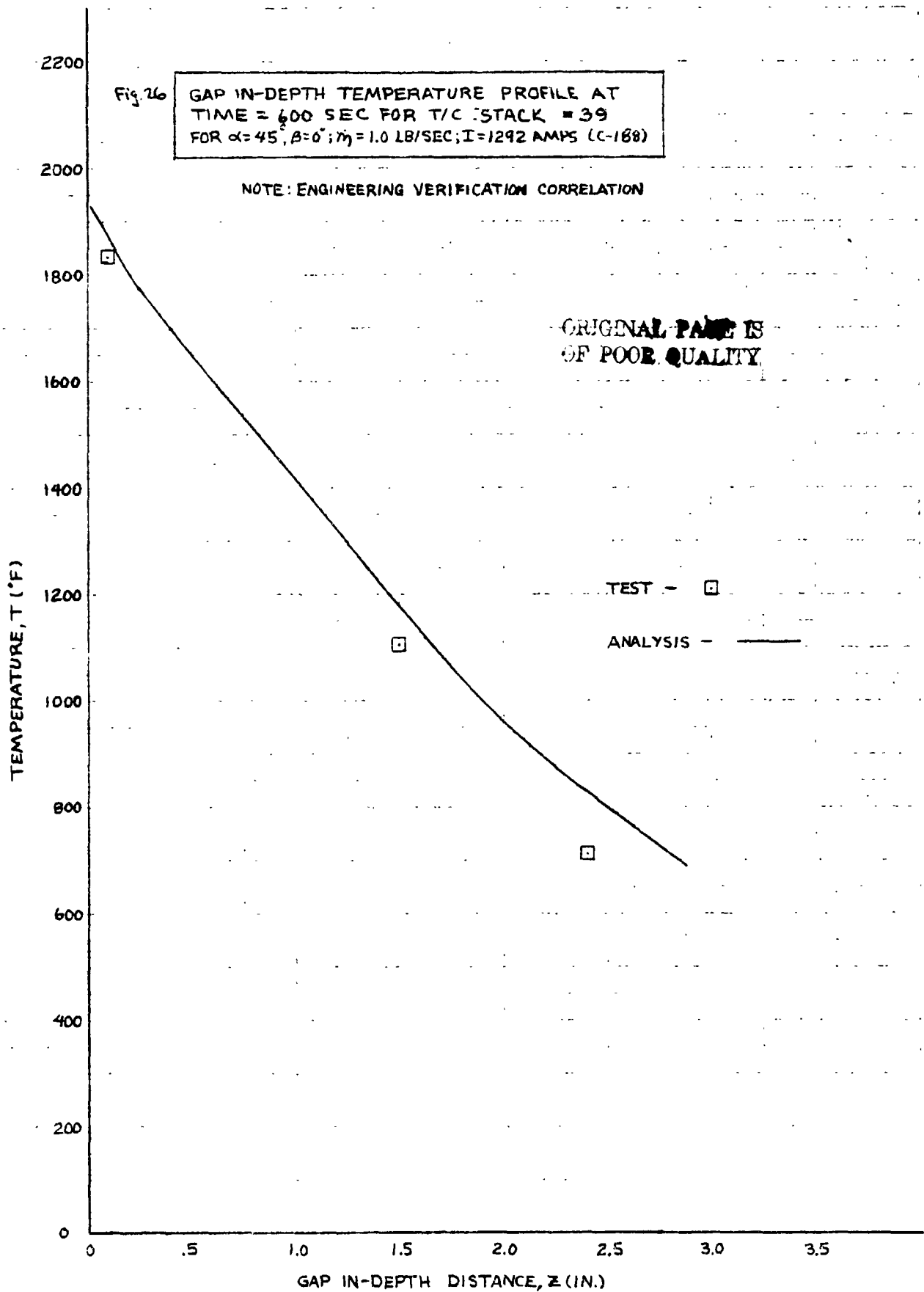
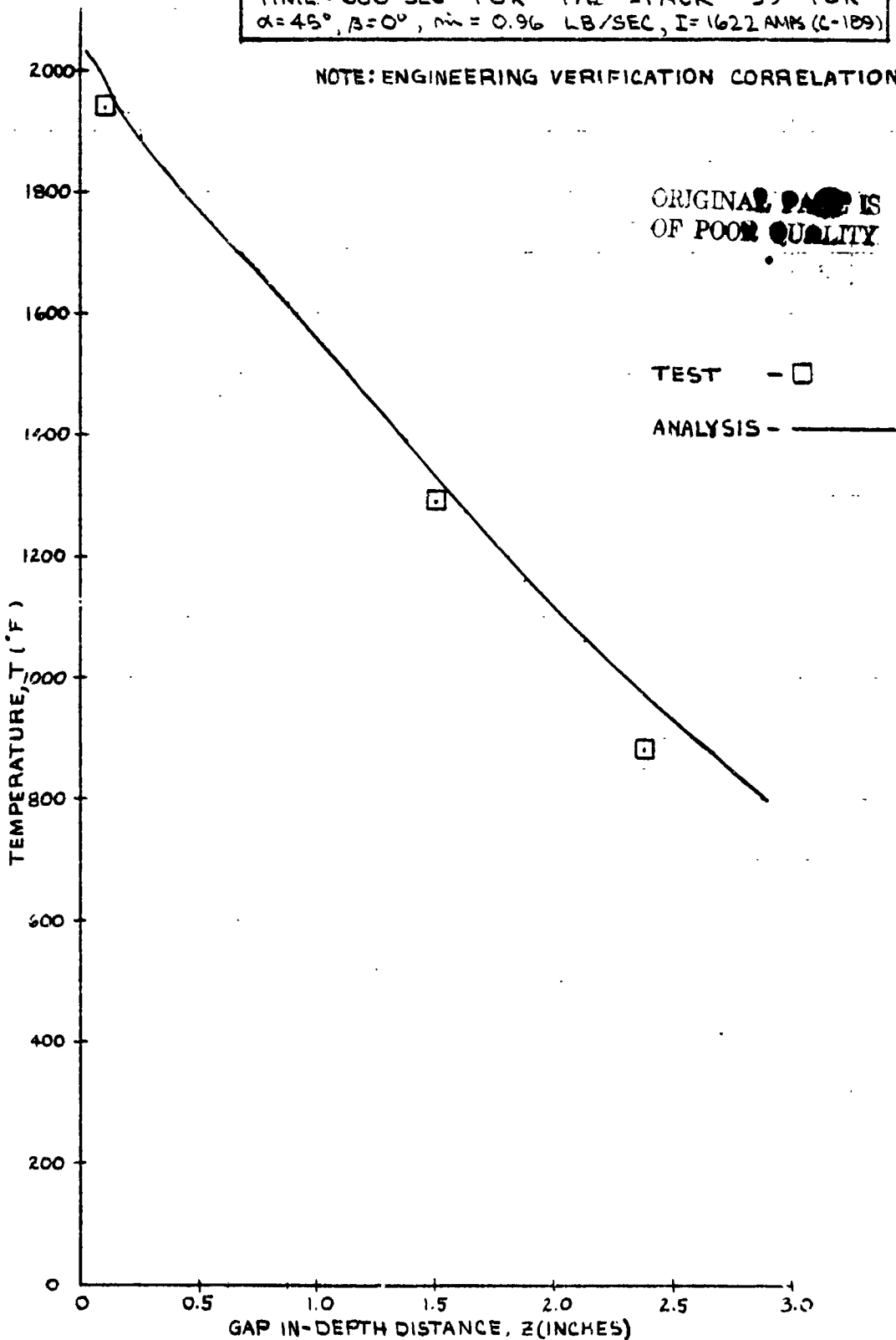
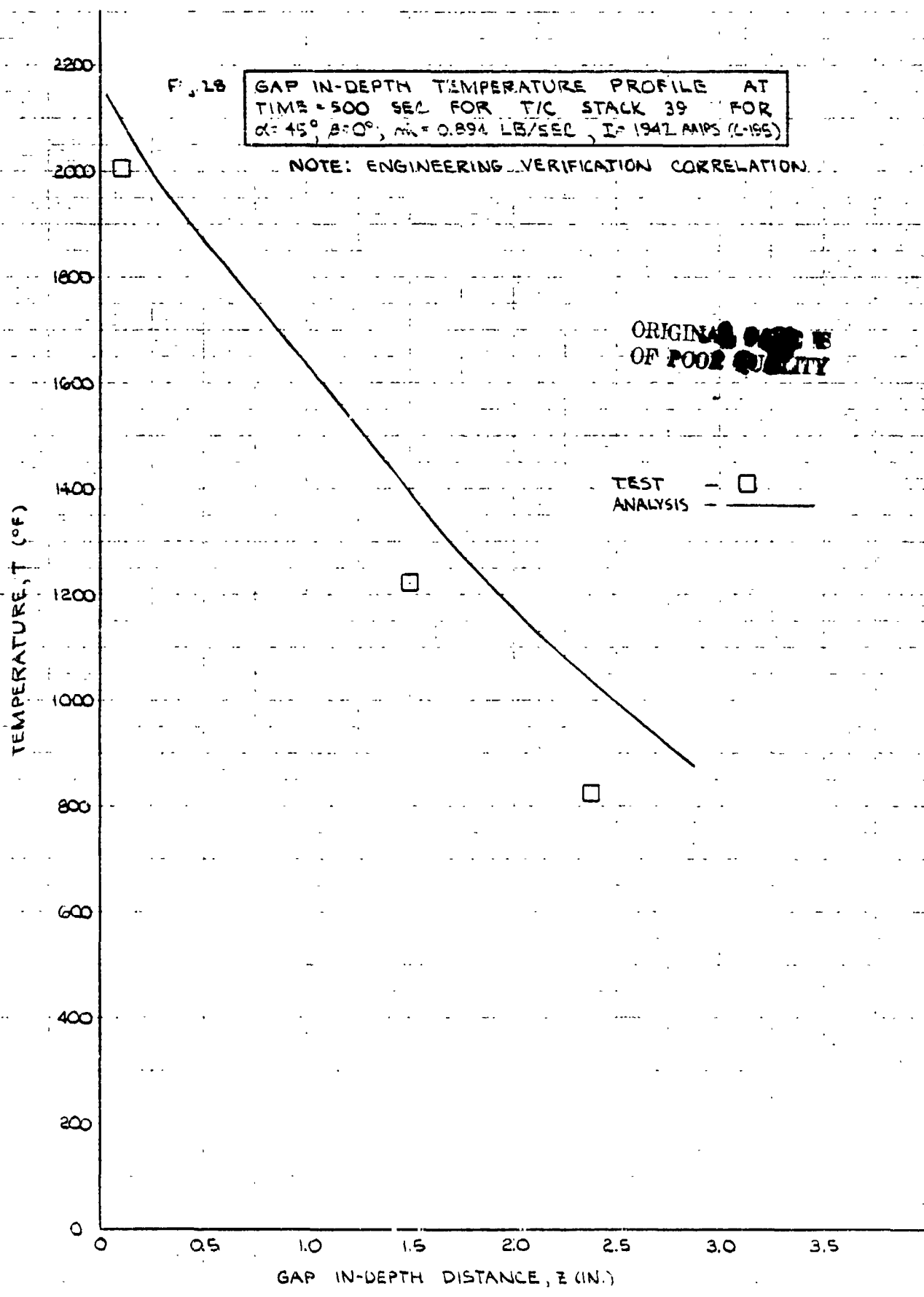


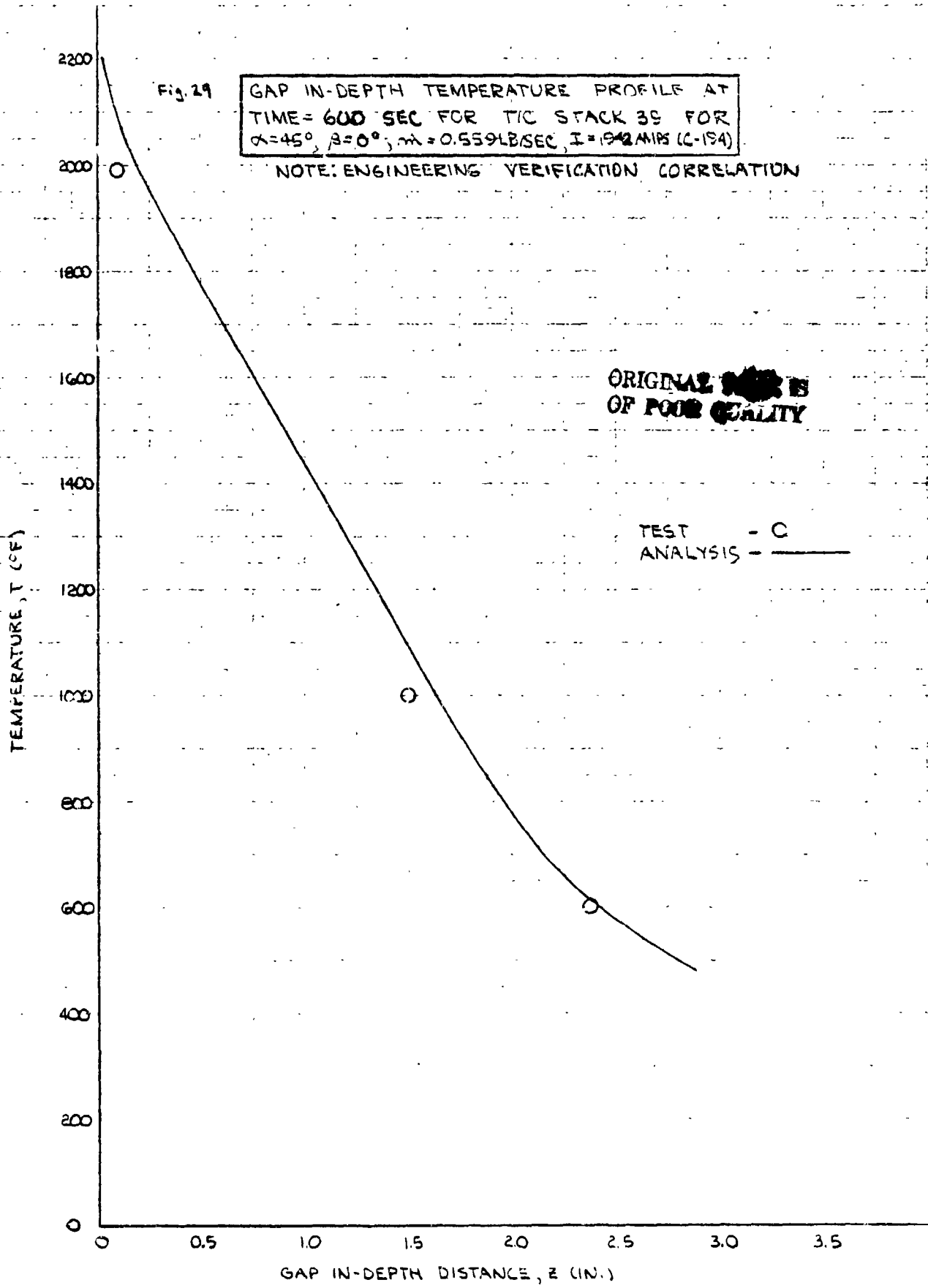
Fig. 27

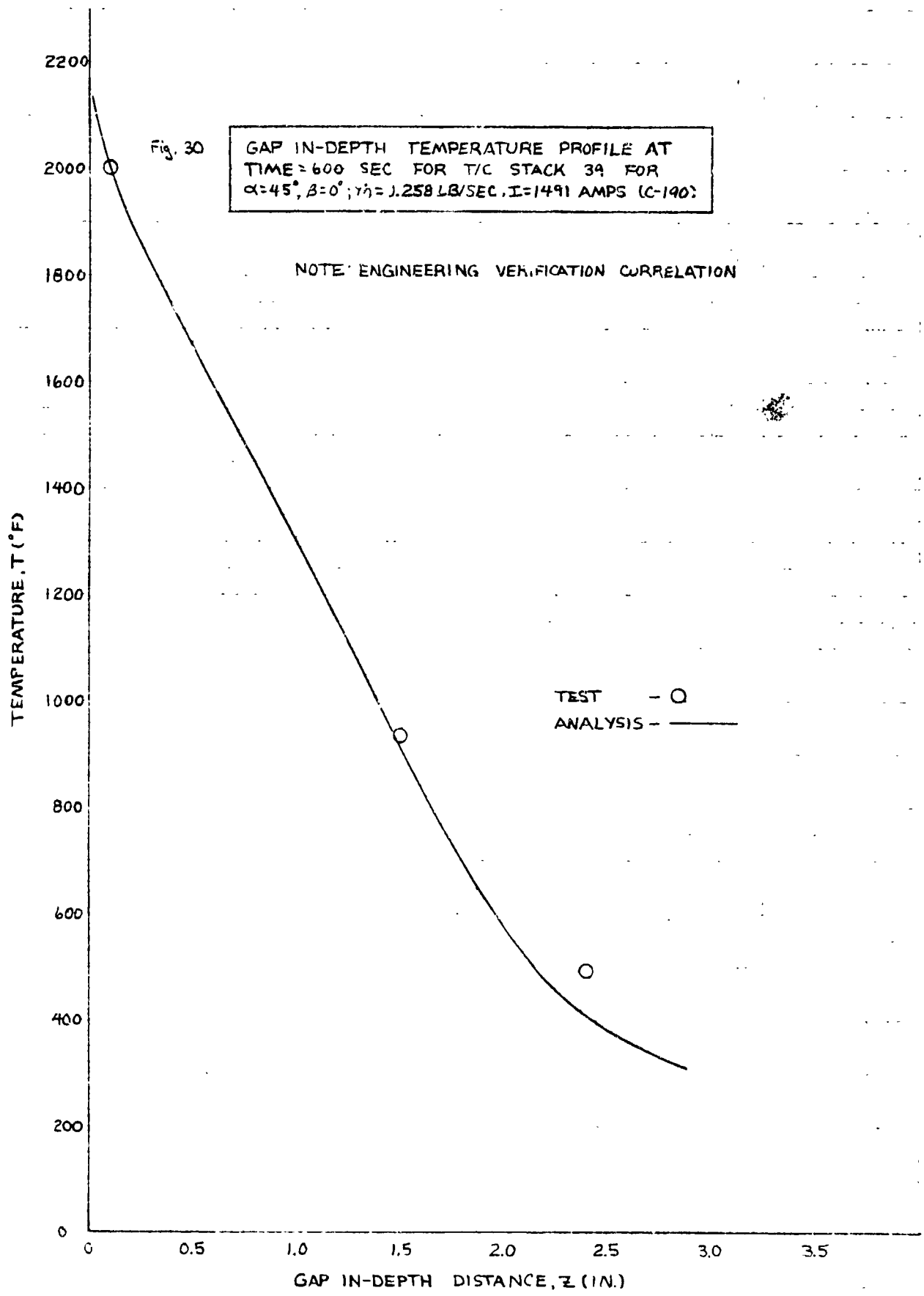
GAP IN-DEPTH TEMPERATURE PROFILE AT  
TIME = 600 SEC FOR T/G STACK 39 FOR  
 $\alpha = 45^\circ$ ,  $\beta = 0^\circ$ ,  $\dot{m} = 0.96$  LB/SEC,  $I = 1622$  AMPS (C-189)

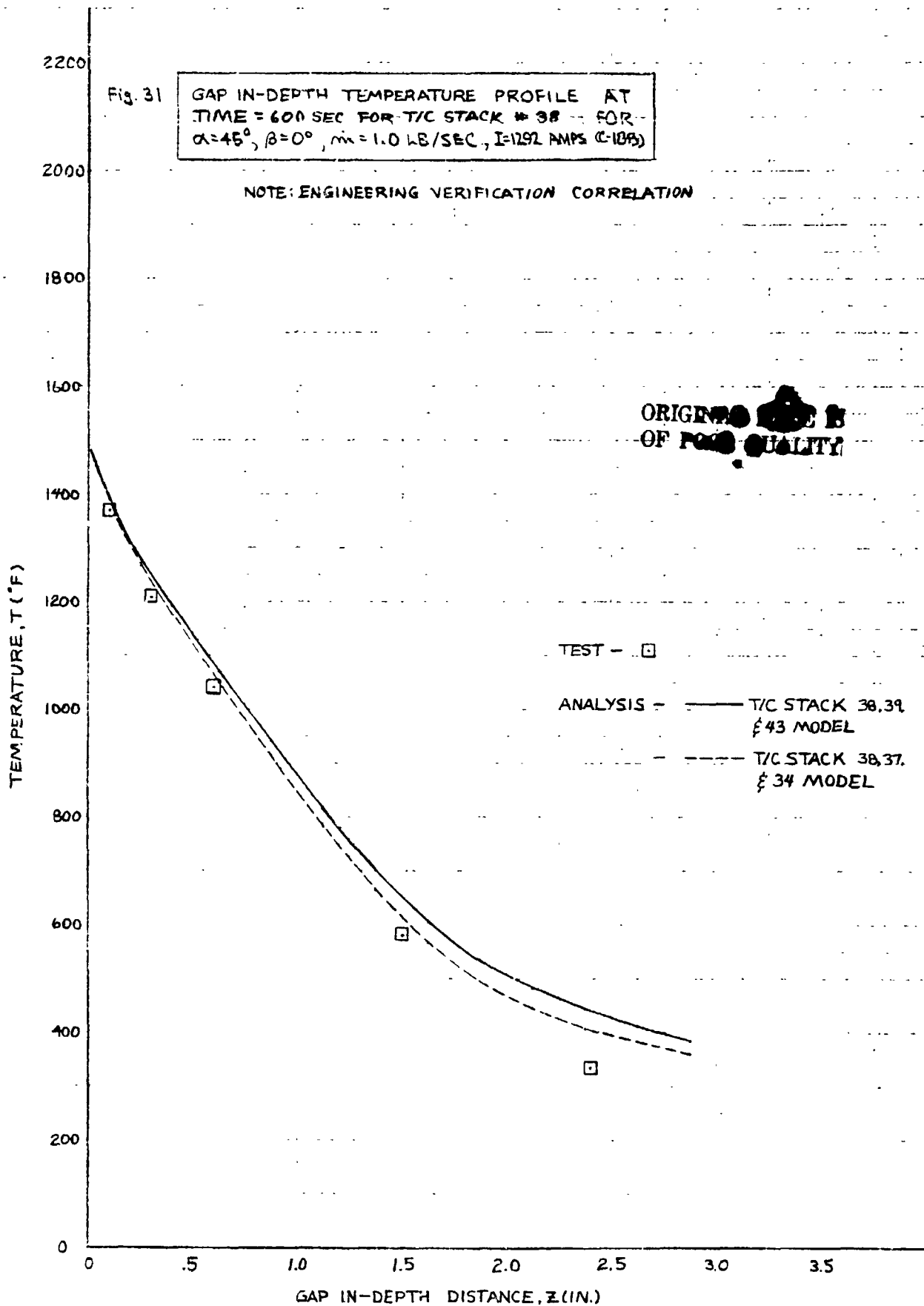
NOTE: ENGINEERING VERIFICATION CORRELATION











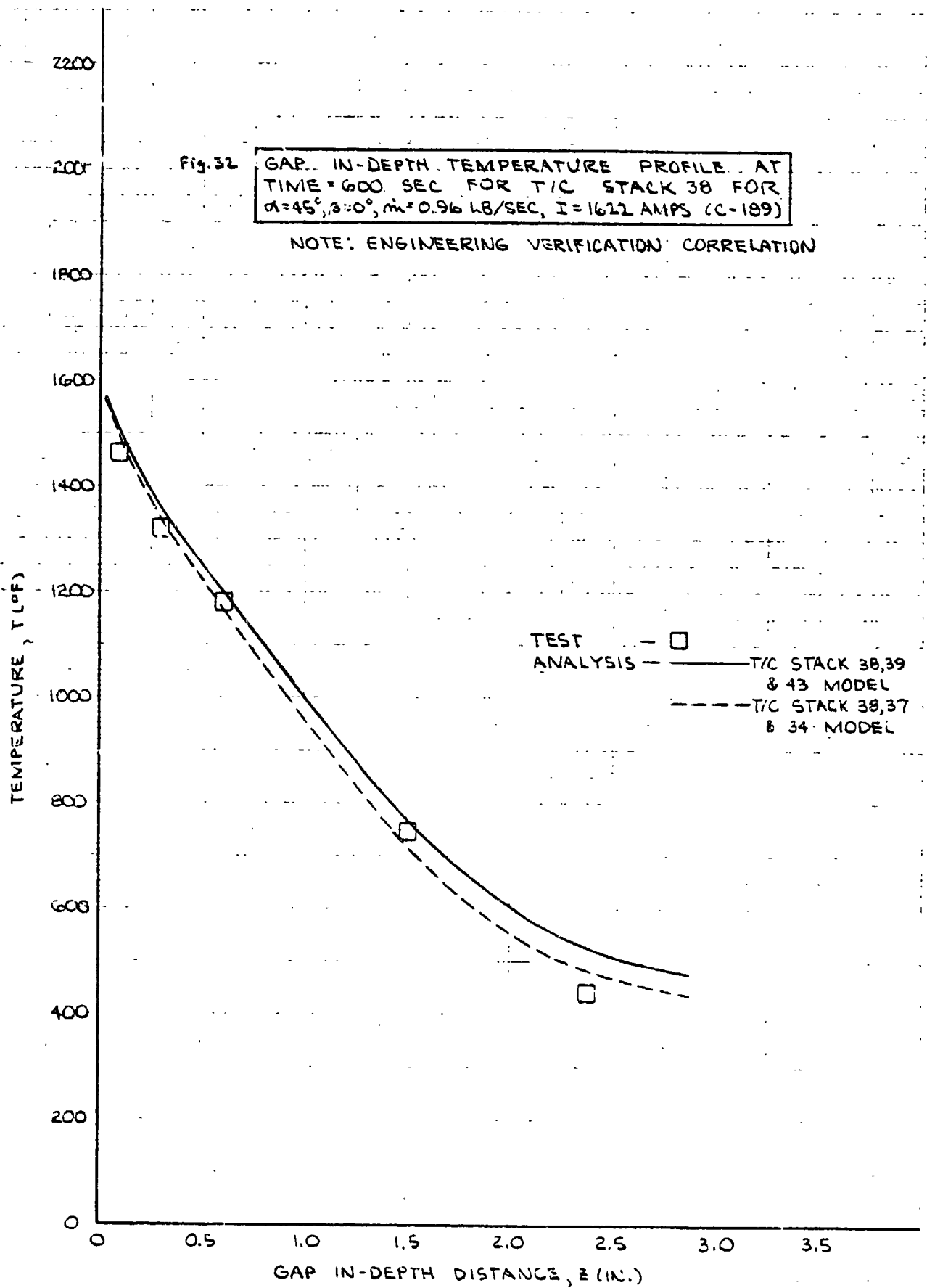
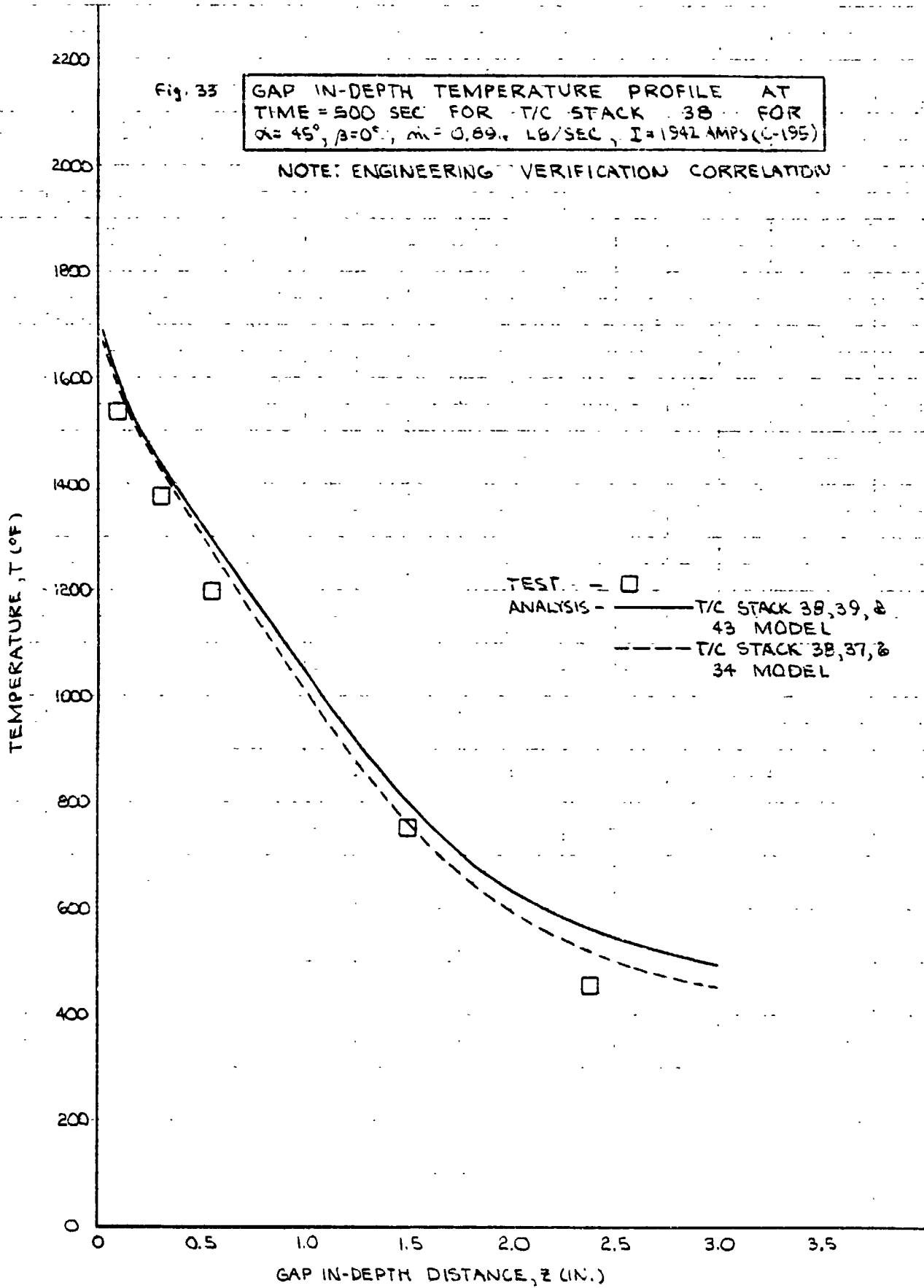
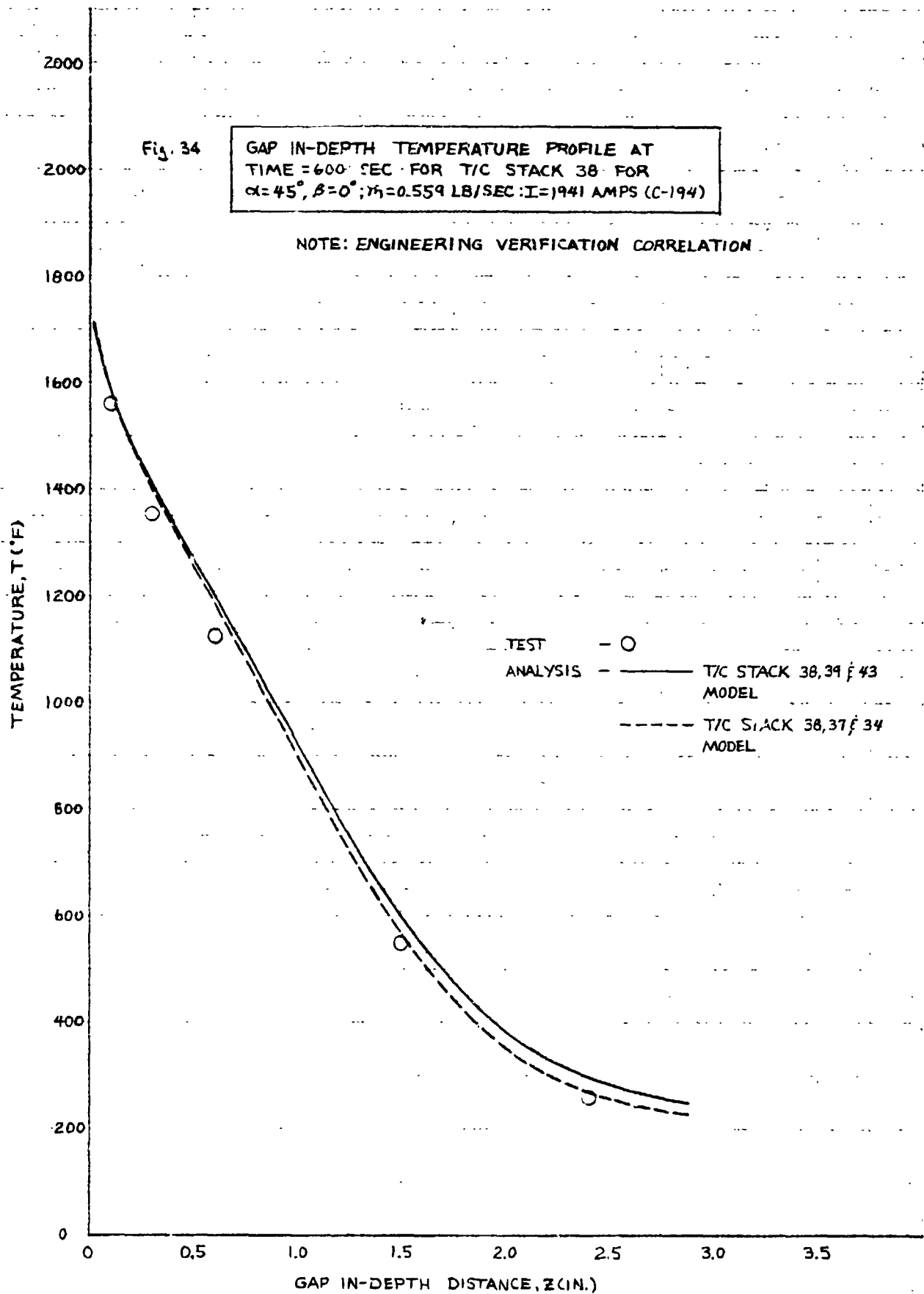


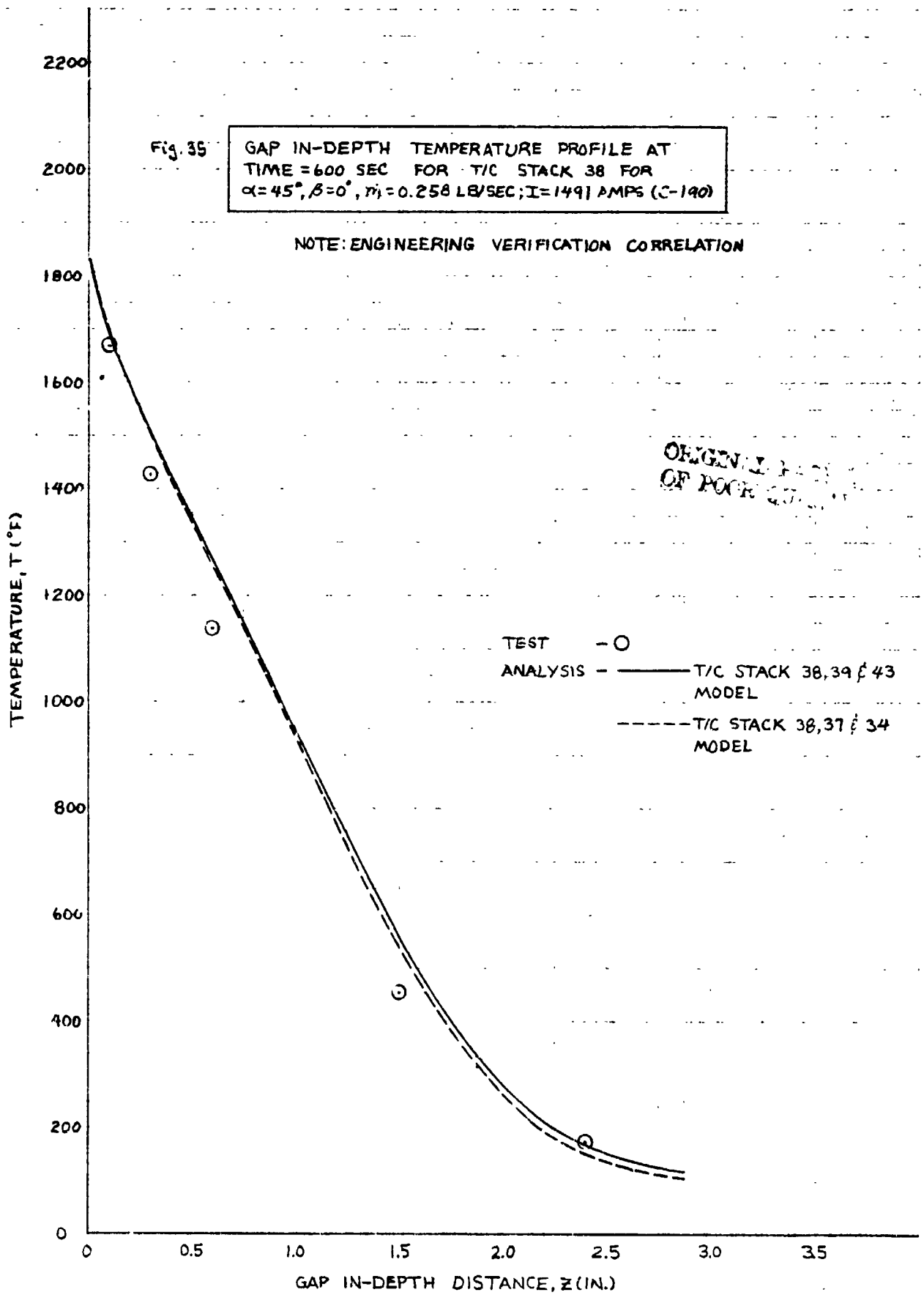
Fig. 33

GAP IN-DEPTH TEMPERATURE PROFILE AT  
TIME = 500 SEC FOR T/C STACK 38 FOR  
 $\alpha = 45^\circ, \beta = 0^\circ, m = 0.89, \text{ LB/SEC}, I = 1942 \text{ AMPS (C-195)}$

NOTE: ENGINEERING VERIFICATION CORRELATION







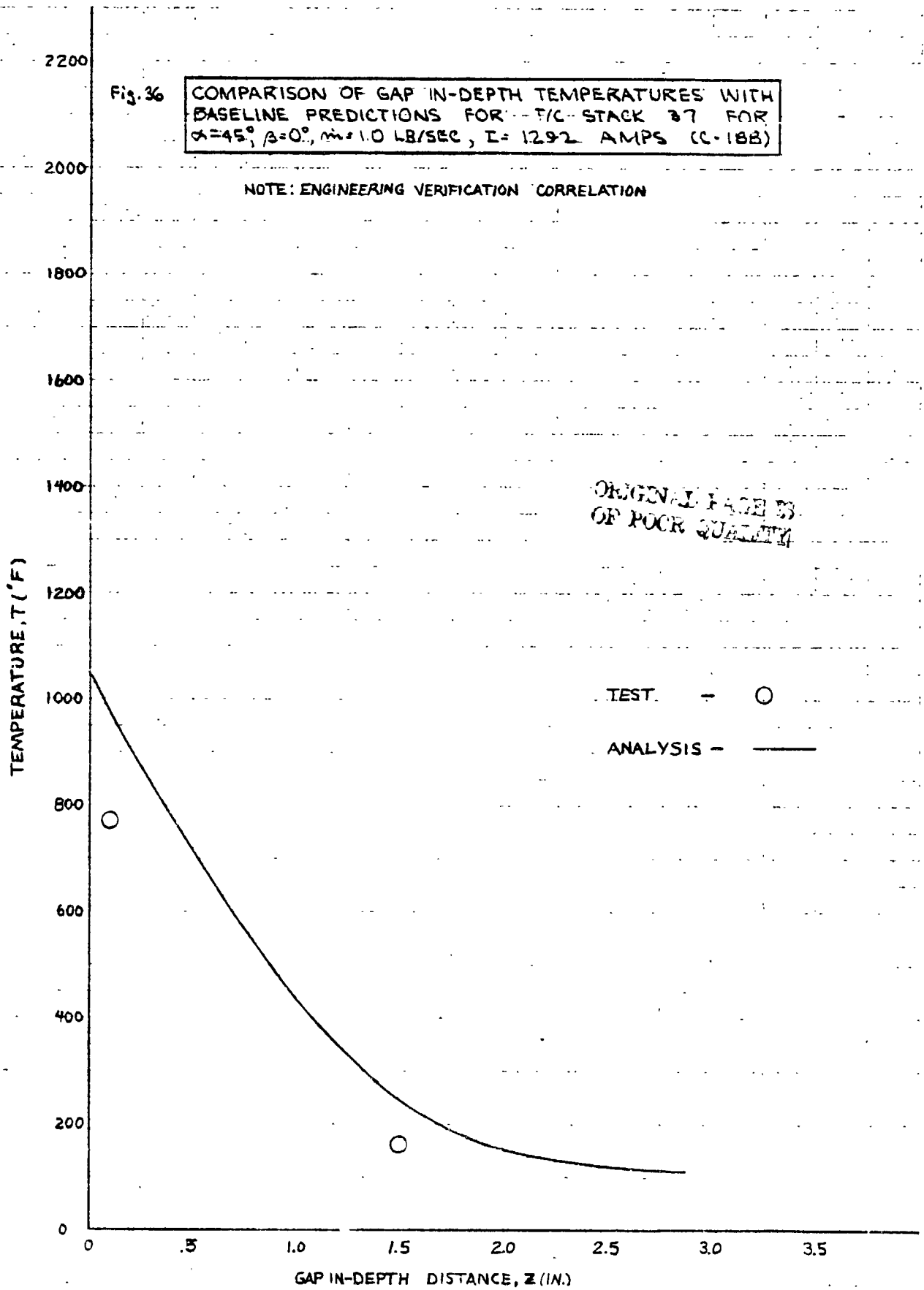


Fig. 37

COMPARISON OF GAP IN-DEPTH TEMPERATURES WITH  
BASELINE PREDICTIONS FOR T/C STACK 37 FOR  
 $\alpha=45^\circ, \beta=0^\circ, \dot{m}=0.96 \text{ LB/SEC}, I=1622 \text{ AMPS (C-189)}$

NOTE: ENGINEERING VERIFICATION CORRELATION

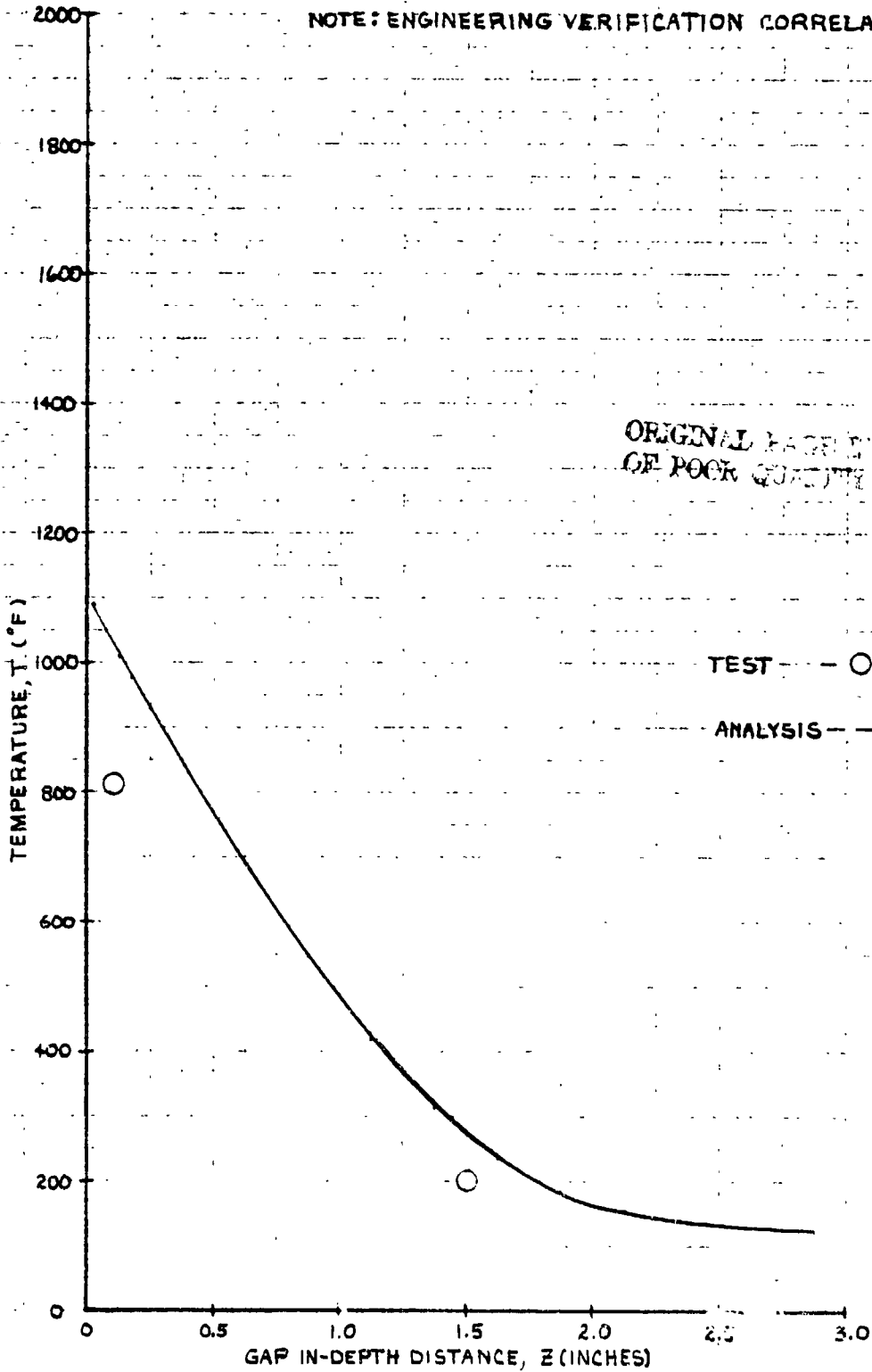


Fig. 38 COMPARISON OF GAP IN-DEPTH TEMPERATURES WITH  
BASELINE PREDICTIONS FOR T/C STACK 37 FOR  
 $\alpha=45^\circ$ ,  $\beta=0^\circ$ ,  $\dot{m} = 0.89$  LB/SEC,  $I = 1942$  AMPS (C-195)

NOTE: ENGINEERING VERIFICATION CORRELATION

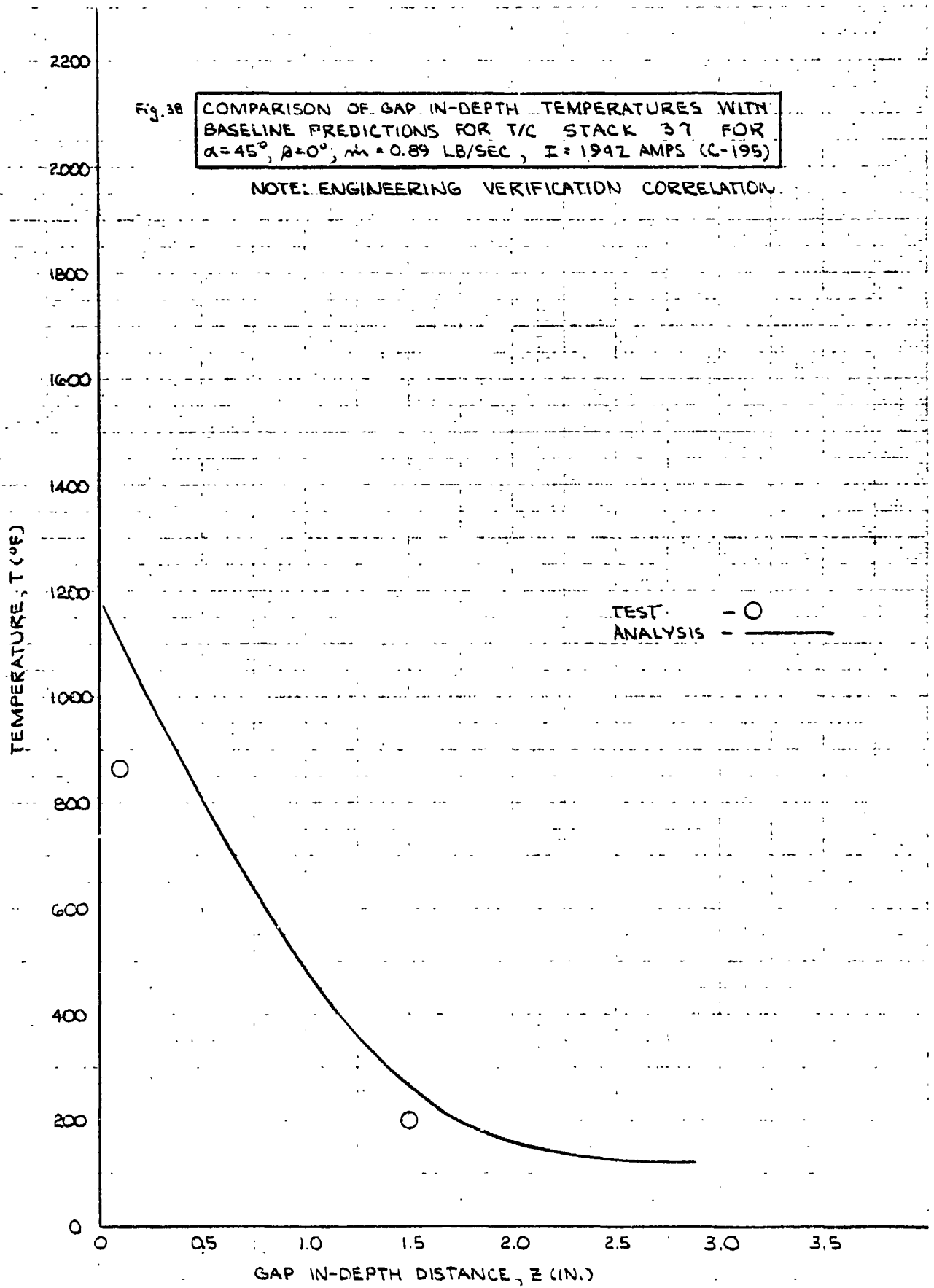


Fig. 39. COMPARISON OF GAP IN-DEPTH TEMPERATURES WITH  
BASELINE PREDICTIONS FOR T/C STACK 37 FOR  
 $\alpha=45^\circ$ ,  $\beta=0^\circ$ ,  $m=0.559$  LB/SEC,  $I=1942$  AMPS (C-194)

NOTE: ENGINEERING VERIFICATION CORRELATION

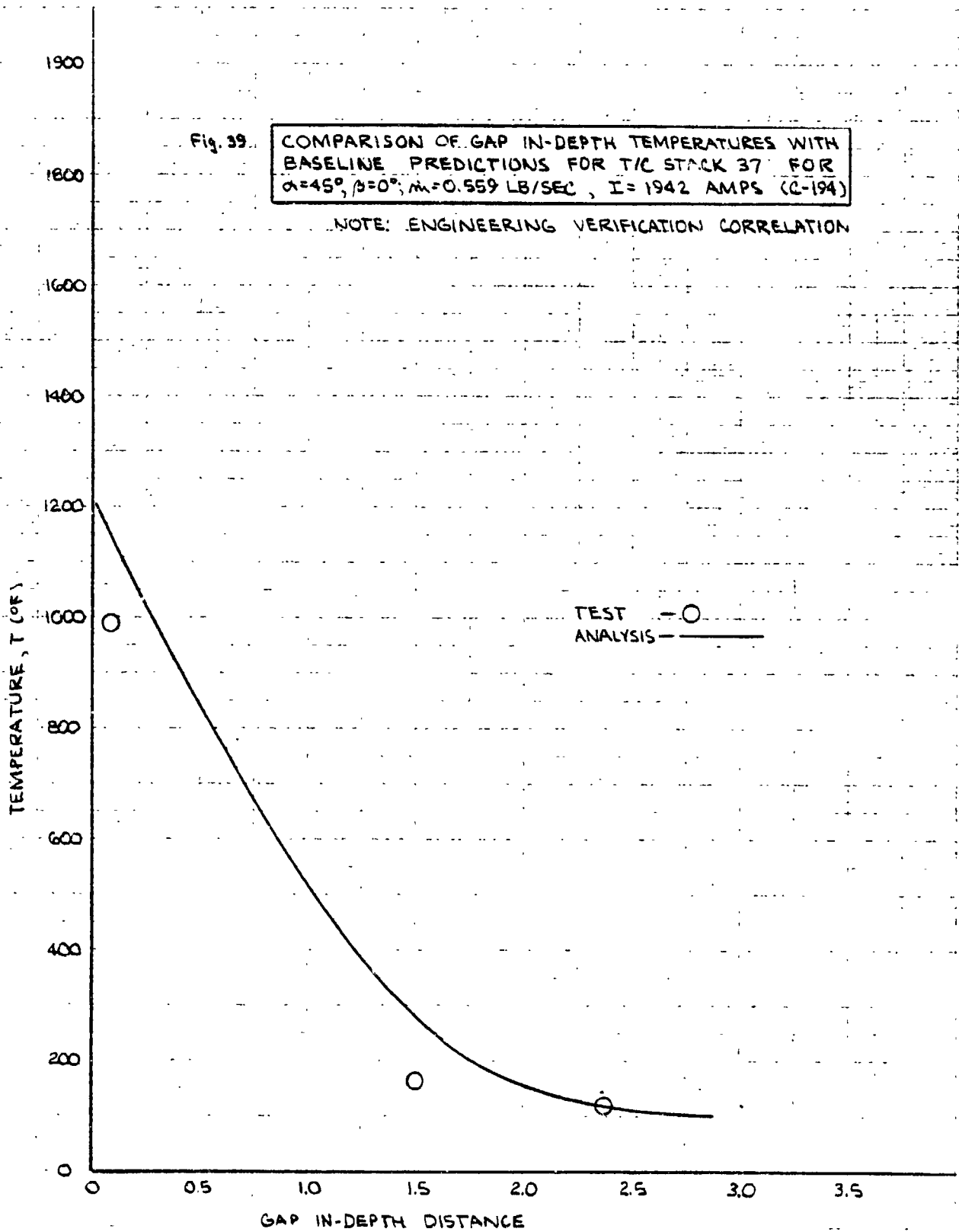
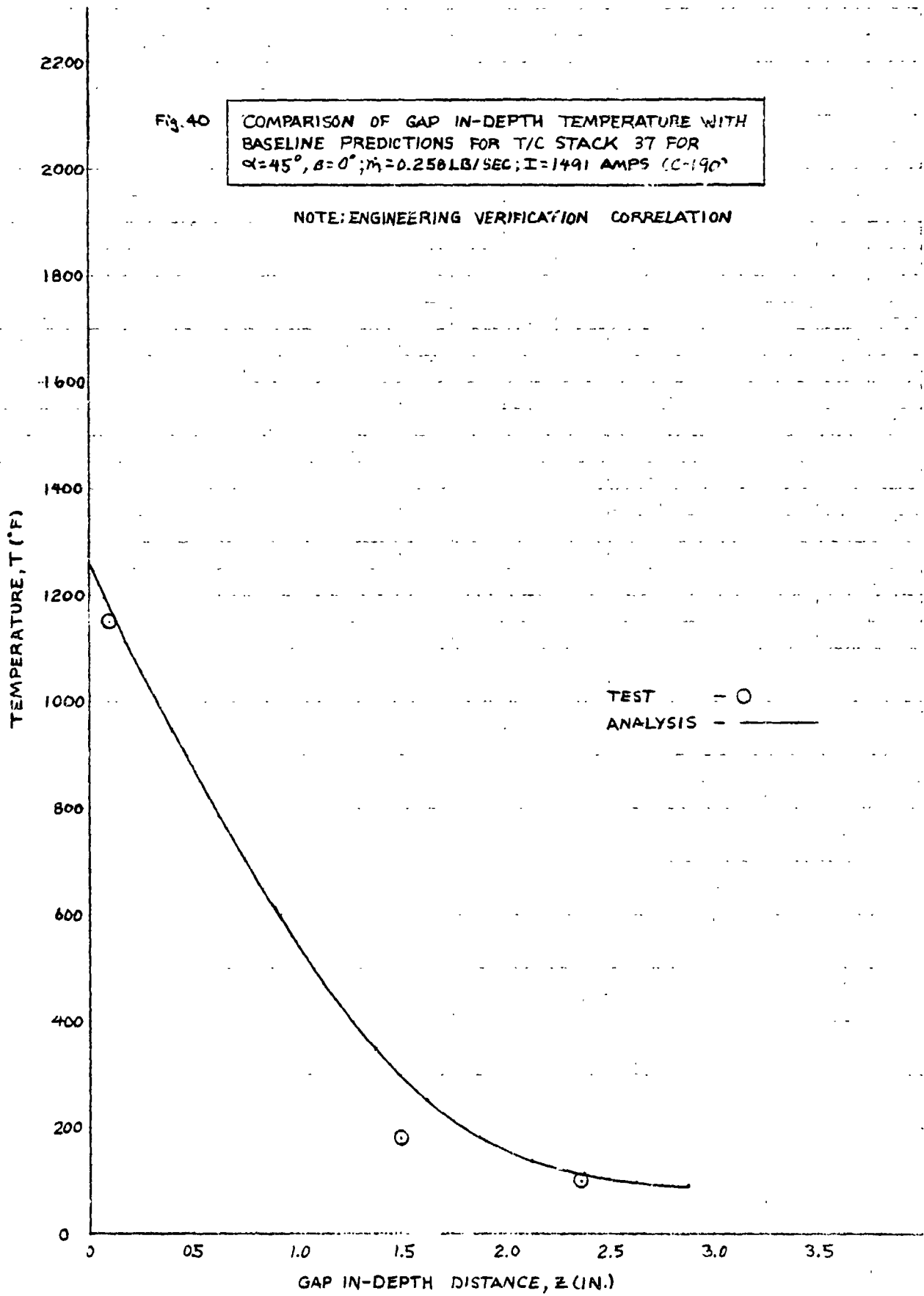


Fig. 40

COMPARISON OF GAP IN-DEPTH TEMPERATURE WITH  
BASELINE PREDICTIONS FOR T/C STACK 37 FOR  
 $\alpha=45^\circ, \beta=0^\circ; \dot{m}=0.250 \text{ LB/SEC}; I=1491 \text{ AMPS (C-190)}$

NOTE: ENGINEERING VERIFICATION CORRELATION



GAP IN-DEPTH TEMPERATURES AS A FUNCTION OF TIME FOR TIC STACK 39 FOR  $\alpha=45^\circ$ ,  $\beta=0^\circ$ ,  $\rho_m=0.894$  LB/SEC,  $I=1942$  AMPS (C-195)

T/C GAP DEPTH  
 24A .1 IN.  
 26A 1.5 IN.  
 27A 2.38 IN.

○ △ ▽

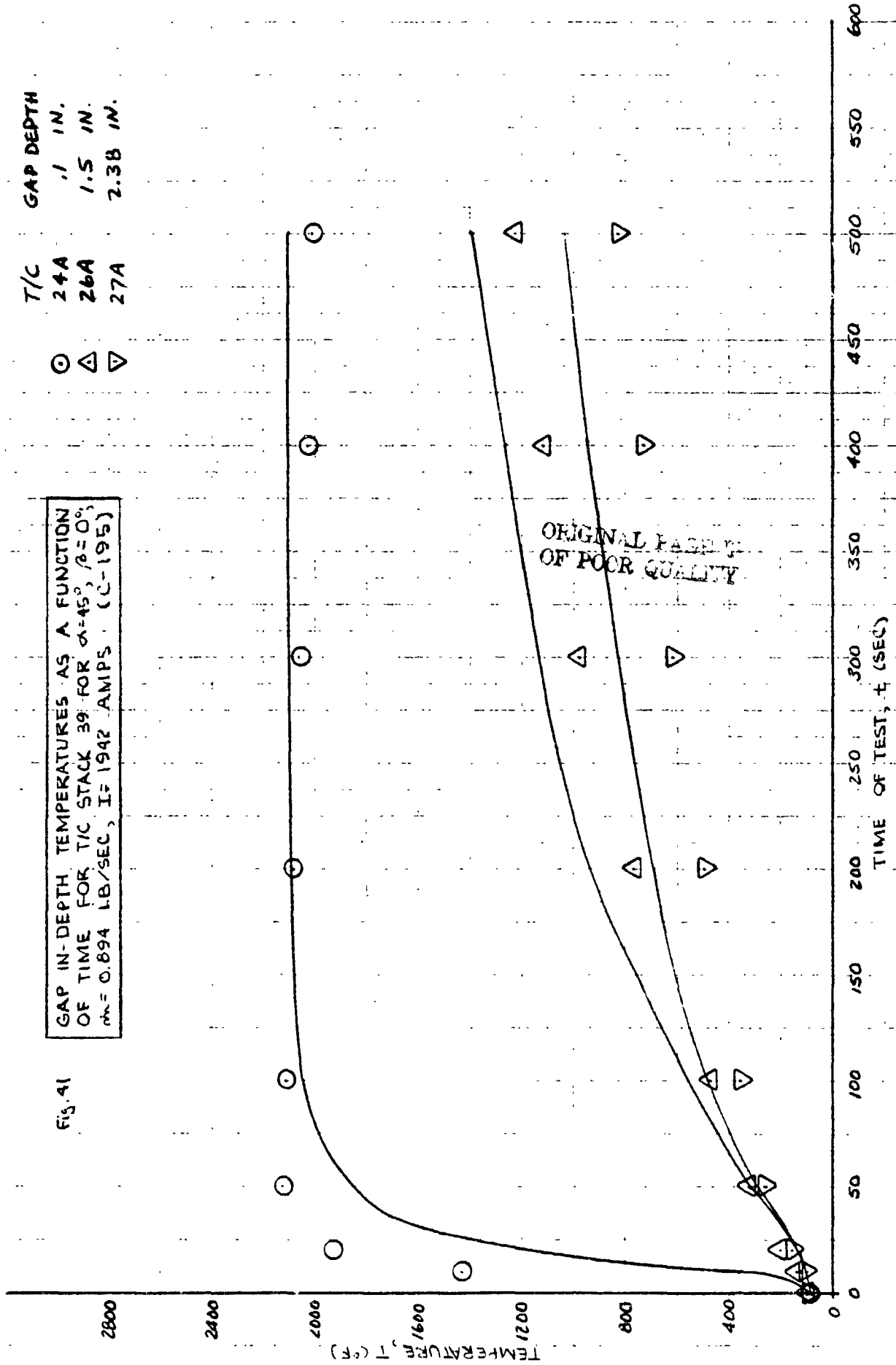


Fig. 41

GAP IN-DEPTH TEMPERATURES AS A FUNCTION OF TIME FOR T/C STACK 39 FOR  $\alpha=45^\circ$ ,  $\beta=0^\circ$ ,  $\dot{m} = 0.559$  LB/SEC,  $I=1491$  AMPS (C-194)

T/C	GAP DEPTH
24A	.1 IN.
26A	1.5 IN.
27A	2.38 IN.

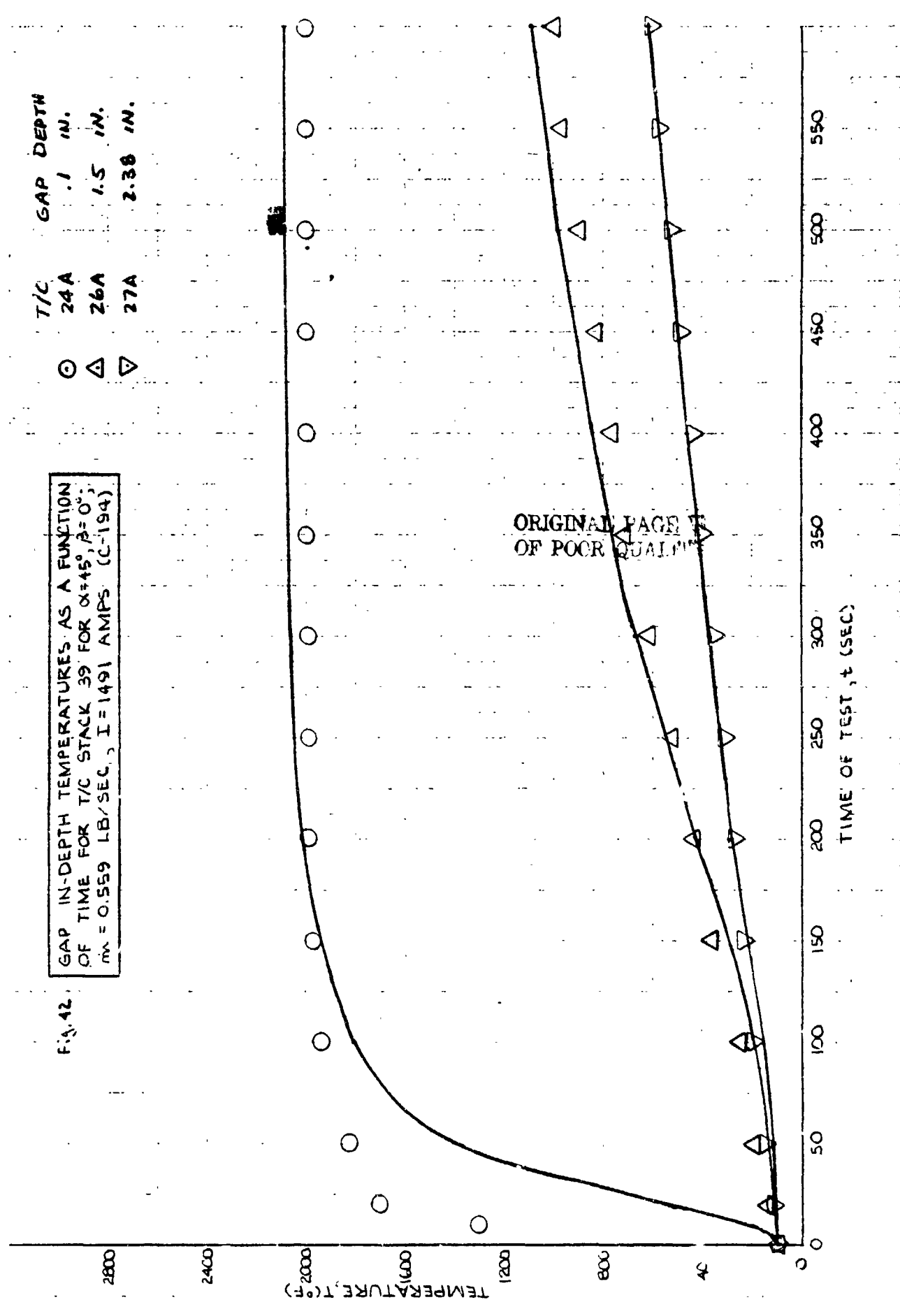


Fig. 42

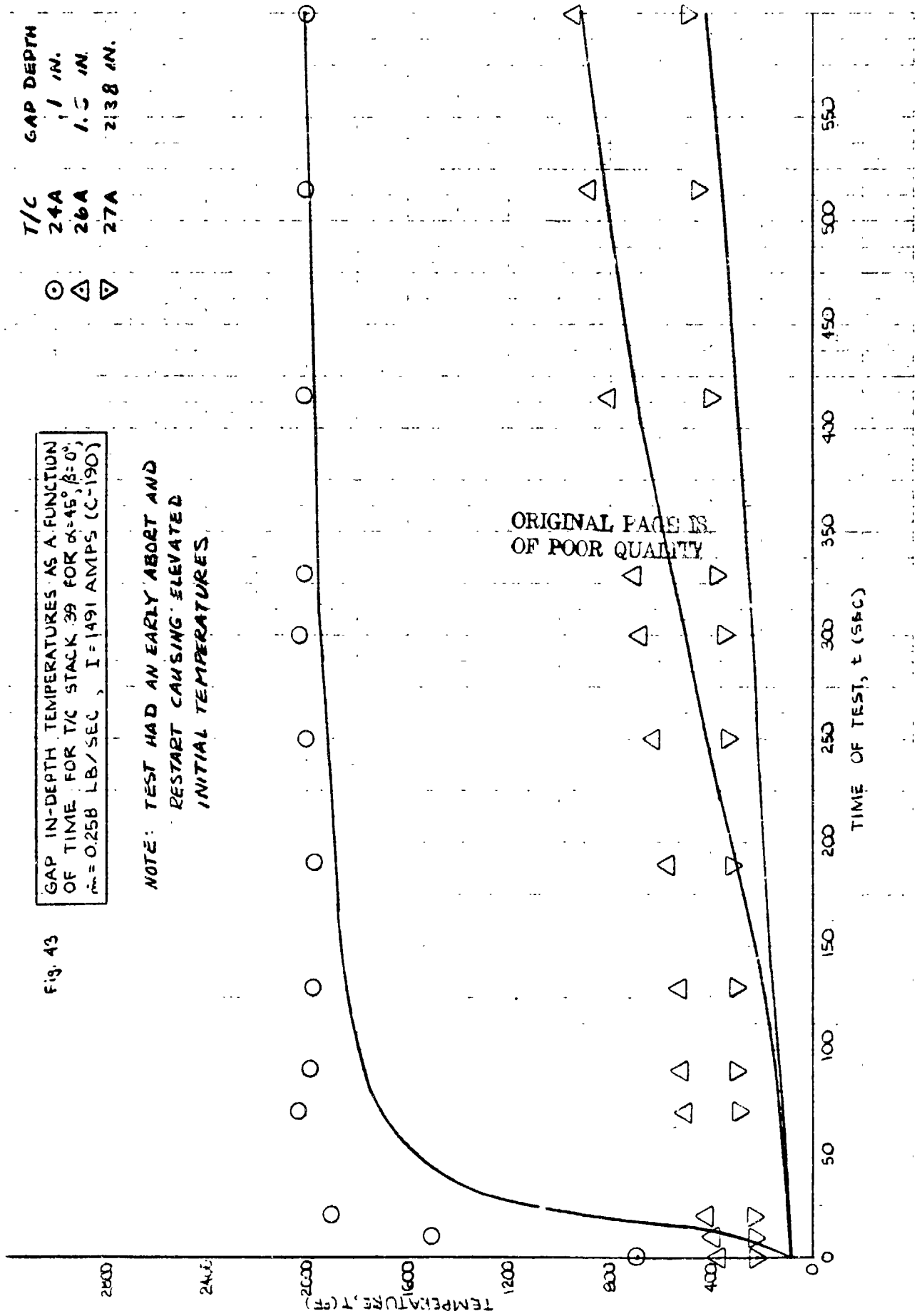
Fig. 43

GAP IN-DEPTH TEMPERATURES AS A FUNCTION OF TIME FOR T/C STACK 39 FOR  $\alpha=45^\circ$ ,  $\beta=0^\circ$ ,  $\dot{m}_c = 0.258$  LB/SEC,  $I = 1491$  AMPS (C-190)

NOTE: TEST HAD AN EARLY ABORT AND RESTART CAUSING ELEVATED INITIAL TEMPERATURES

T/C GAP DEPTH  
 24A 1 IN.  
 26A 1.5 IN.  
 27A 2.38 IN.

○ △ ▽



ORIGINAL PAGE IS OF POOR QUALITY

GAP IN-DEPTH TEMPERATURES AS A FUNCTION OF TIME FOR T/C STACK 38 FOR  $\alpha=15^\circ$ ,  $\beta=0^\circ$ ,  $M=0.694$  LB/SEC,  $I=1942$  AMPS (C-195)

T/C	GAP DEPTH
19A	.1 IN.
20A	.3 IN.
21A	.6 IN.
22A	1.5 IN.
23A	2.38 IN.

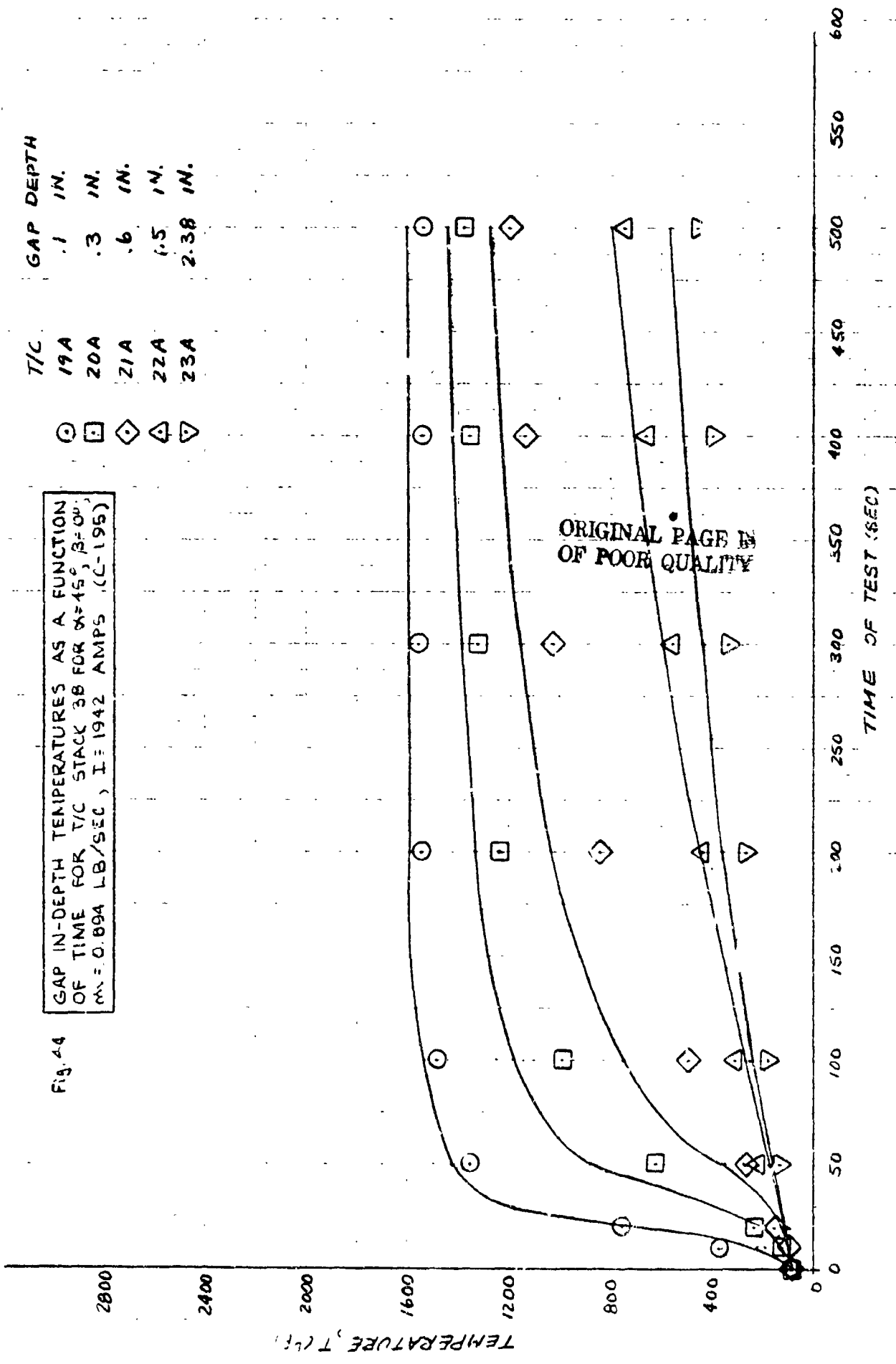
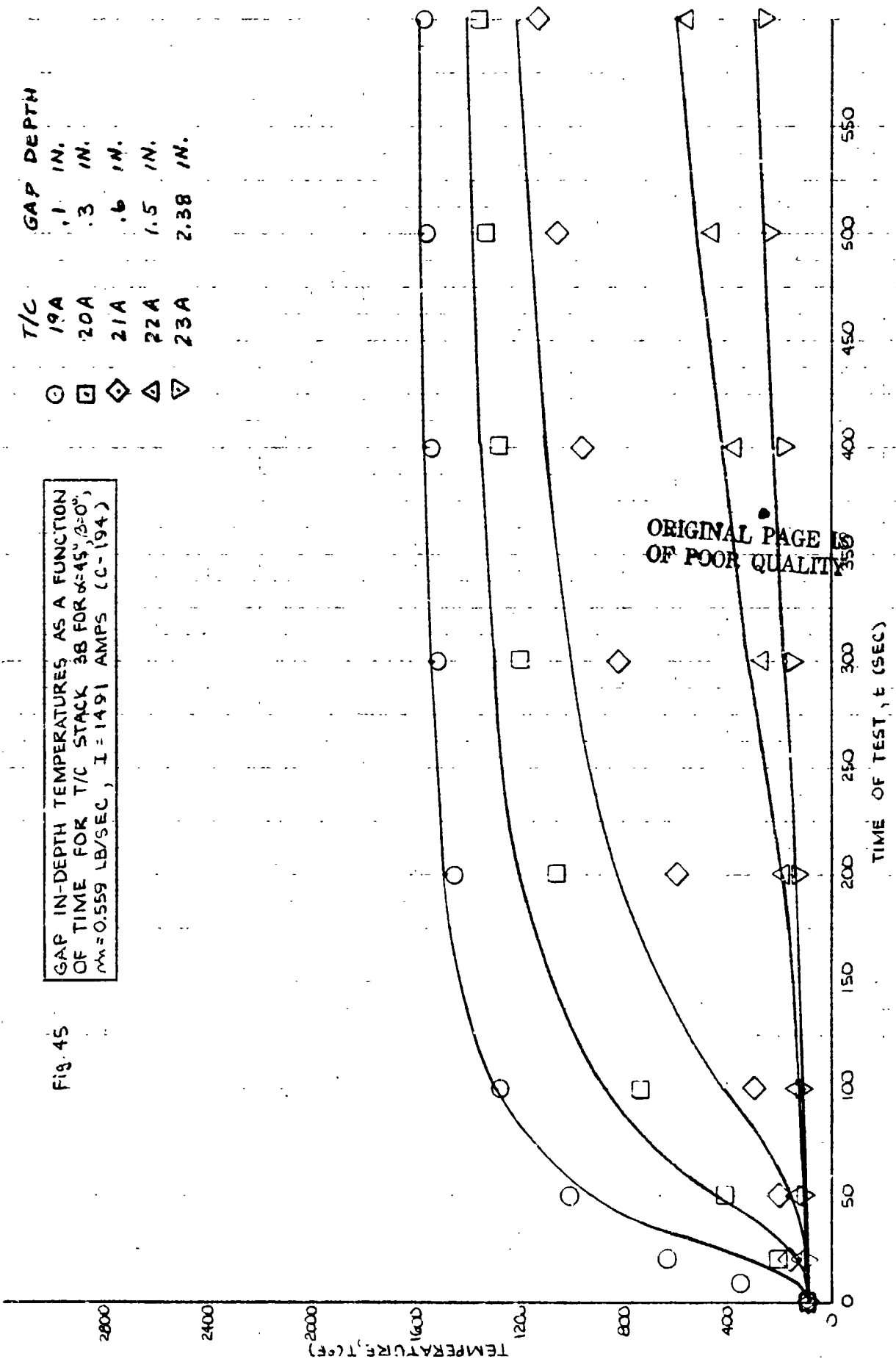


Fig. 44

Fig. 45  
 GAP IN-DEPTH TEMPERATURES AS A FUNCTION  
 OF TIME FOR T/C STACK 3B FOR  $\alpha=45^\circ$ ,  $\beta=0^\circ$ ,  
 $m_0=0.559$  LB/SEC,  $I=1491$  AMPS (C-194)

T/C	GAP DEPTH
19A	.1 IN.
20A	.3 IN.
21A	.6 IN.
22A	1.5 IN.
23A	2.38 IN.



GAP IN-DEPTH TEMPERATURES AS A FUNCTION OF TIME FOR T/C STACK 36 FOR  $\alpha=45^\circ$ ,  $\beta=0^\circ$ ,  $m=0.258$  LB/SEC,  $I=1491$  AMPS (C-190)

T/C	GAP DEPTH
19A	.1 IN.
20A	.3 IN.
21A	.6 IN.
22A	1.5 IN.
23A	2.38 IN.

